lubricants

MDPI

Article

Experimental Investigation of Lubrication Effects in High-Feed Face Milling Using DOE-Based Cutting Force and Surface Analysis

Gyula Varga *, István Sztankovics * and Antal Nagy

Institute of Manufacturing Science, Faculty of Mechanical Engineering and Informatics, University of Miskolc, H-3515 Miskolc, Hungary

* Correspondence: gyula.varga@uni-miskolc.hu (G.V.); istvan.sztankovics@uni-miskolc.hu (I.S.)

Abstract

High-feed face milling is widely adopted in industry for its productivity advantages, especially when machining medium carbon steels. However, the combined effects of lubrication regimes on both the cutting forces and surface quality remain insufficiently explored, creating a research gap in optimizing process parameters for improved performance. This study presents an experimental investigation into the effects of lubrication on cutting forces and surface topography during the high-feed face milling of C45 steel. Using a design of experiments (DOE) approach, eight distinct machining setups were developed by varying the cutting speed, depth of cut, and feed per tooth. Each setup was tested under two lubrication conditions: with flood coolant and under dry machining. Cutting forces in the X, Y, and Z directions were recorded using a dynamometer, while the post-machining surface quality was evaluated using 3D areal surface topography measurements. The results revealed that feed per tooth was the primary factor affecting both the cutting forces and surface roughness, with depth of cut having a moderate effect and cutting speed a minor influence. Flood lubrication reduced the peak forces, stabilized force fluctuations, and improved surface uniformity, particularly in the valley depths and skewness parameters. This work provides (i) a combined analysis of cutting forces and surface topography under high-feed milling, (ii) quantitative evidence of lubrication effects on force and surface consistency, and (iii) identification of dominant process parameters for optimization, offering practical guidance for enhancing productivity, surface quality, and tribological performance in high-feed milling operations.

Keywords: cutting force; DOE; dry machining; face milling; high-feed machining; lubrication; roughness; surface topography

Check for updates

Received: 31 August 2025
Revised: 13 October 2025
Accepted: 16 October 2025
Published: 3 February 2026

Copyright: © 2026 by the authors. Licensee MDPI, Basel, Switzerland. This article is an open access article distributed under the terms and conditions of the Creative Commons Attribution (CC BY) license.

1. Introduction

The primary objectives of modern manufacturing are to produce components efficiently while maintaining high dimensional accuracy, surface quality, and structural integrity. At the same time, the industry is under increasing pressure to reduce energy consumption, minimize material waste, extend tool life, and ensure environmentally responsible processes [1–3]. Machining operations, particularly milling, play a central role in achieving these objectives, as they are widely applied for shaping, finishing, and preparing parts for assembly [4,5]. Success in these operations depends heavily on understanding the cutting forces, heat generation, chip formation, and tool–workpiece interactions. These

factors not only determine the immediate productivity, but also the long-term component performance as they directly affect the surface integrity, residual stresses, and potential microstructural alterations. Therefore, a comprehensive knowledge of the forces acting during machining and the resulting surface characteristics is essential for optimizing processes and achieving predictable outcomes [6,7].

Lubrication has long been recognized as a key strategy to improve machining performance [8,9]. Its primary roles are to reduce friction at the interface between the cutting tool and workpiece, dissipate heat generated during cutting, and prevent or slow down tool wear. By reducing friction, lubricants minimize energy losses in the system, allowing for more stable cutting conditions and consistent material removal. The effectiveness of lubrication depends on its mechanism of action, which can include hydrodynamic, boundary, and mixed lubrication regimes [10]. In hydrodynamic lubrication, a fluid film completely separates the tool and workpiece, reducing direct contact and associated wear. Boundary lubrication relies on surface films formed by additives, which can adhere to the tool and workpiece surfaces to reduce metal-to-metal contact. Mixed lubrication combines aspects of both, providing the partial separation of surfaces while still supporting load transfer. These mechanisms, whether applied via flood cooling, minimal quantity lubrication, or other strategies, have distinct impacts on the process performance. Proper lubricant selection and application are therefore crucial in minimizing the cutting forces, extending tool life, and ensuring consistent surface quality across multiple operations [11,12].

Dry machining, in contrast, eliminates lubricants entirely, offering clear environmental and economic advantages such as reduced fluid consumption, lower disposal requirements, and simplified workpiece handling [13–15]. However, operating without lubrication presents significant challenges. The absence of cooling and lubricating films leads to elevated cutting temperatures [16], which can accelerate tool wear [17] and increase thermal stresses on the workpiece [18]. Additionally, friction between the tool and material rises, potentially altering chip formation, increasing the cutting forces, and degrading the surface finish [19]. Despite these drawbacks, dry machining remains attractive in high-speed or low-volume scenarios where the management of cutting fluids is impractical or economically unfeasible. Optimizing dry machining conditions requires the careful selection of cutting parameters, tool geometry, and process monitoring strategies to mitigate the negative effects of elevated heat and friction [20–22].

Face milling is one of the most commonly used machining processes, particularly for producing flat surfaces or removing material over large areas [23,24]. In this process, multiple cutting edges engage the workpiece simultaneously, distributing the cutting load across several teeth and enabling higher material removal rates with relatively low forces per edge. This characteristic makes face milling an efficient choice for medium and large workpieces, where the uniform surface quality and dimensional consistency are essential. However, despite its advantages, face milling is highly sensitive to the cutting parameters, tool geometry, and lubrication. Variations in feed, speed, or depth of cut can significantly influence the cutting forces, surface topography, and tool wear. Additionally, the combination of tool rake angle, major cutting edge angle, insert nose radius, and the number of active cutting edges determines the engagement mechanics, chip formation, and surface pattern. Achieving the optimal performance in face milling therefore requires a general understanding of the relationship between the cutting parameters, tool geometry, lubrication, and material behavior.

High-feed milling represents a specialized subset of milling operations designed to maximize productivity by using a large feed per tooth while maintaining a shallow depth of cut [25–27]. This approach allows for fast material removal while keeping the cutting forces per tooth relatively low, reducing the overall energy input and enabling higher

machining efficiency. High-feed strategies are particularly valuable in industries that demand high-volume production such as automotive, aerospace, and mechanical component manufacturing. When applied to medium carbon steels, high-feed milling can significantly enhance the productivity and shorten cycle times. However, high-feed machining introduces unique challenges [28,29]. The low depth of cut, while reducing the per-tooth load, also makes the process more sensitive to vibrations, deflections, and tool chatter. These dynamic effects can lead to inconsistent surface quality, dimensional deviations, and accelerated tool wear if not properly controlled. Moreover, the thermal effects are amplified in high-feed operations because heat generated by friction is concentrated in a smaller contact area. Managing these challenges requires the careful selection of feed rates, cutting speeds, and tool geometries as well as consideration of the lubrication and cooling strategies. Lubrication plays a particularly important role in high-feed milling. While high-feed operations reduce the per-tooth cutting forces, the low depth of cut and high feed can increase the influence of friction and heat at the tool–workpiece interface. The application of a coolant or lubricant film mitigates these effects by providing a thermal sink and reducing friction. Lubricants also contribute to more stable cutting forces and consistent chip formation, which are essential for maintaining the surface quality under high-feed conditions. Additionally, the interaction between tool geometry and lubrication affects the formation of tribo-films, micro-hydrodynamic behavior, and boundary layer effects, all of which influence the machining process at both the macro- and microscales. Properly applied lubrication can therefore enhance process stability, prolong tool life, and improve surface integrity, even in aggressive high-feed conditions.

Recent advances in measurement and monitoring technologies have increased the understanding of high-feed milling and lubrication effects. Three-component dynamometers allow for the accurate measurement of tangential, axial, and radial cutting forces, providing detailed insight into the mechanics of the cutting process [30–32]. Surface topography measurement systems, such as 3D optical profilers, enable the quantitative assessment of surface roughness, waviness, and patterns induced by cutting [33–35]. These tools allow researchers and practitioners to correlate process conditions, such as the feed per tooth, cutting speed, depth of cut, and lubrication, with measurable outcomes in forces, surface quality, and tool wear. Integrating these measurements with a systematic experimental design, such as a design of experiments (DOE) approach [36,37], enables a controlled and reproducible evaluation of the process parameters and their interactions. Despite significant research in machining and lubrication, there remains a gap in the literature concerning comprehensive studies of the high-feed face milling of medium carbon steels under both dry and lubricated conditions [38,39]. Several recent studies have already investigated the simultaneous evaluation of cutting forces and surface quality in milling operations including under different lubrication regimes and for various materials. For example, many studies [40–43] have demonstrated correlations between mechanical tool loads and surface integrity in diverse milling contexts. However, most of these works focused on either advanced alloy steels, hardened materials, or general milling strategies, and often did not systematically compare the combined effects of dry and flood lubrication, specifically in the high-feed face milling of medium carbon steels such as C45. Furthermore, while the relationships between process parameters, cutting forces, and surface roughness are well-established, there remains a lack of comprehensive, quantitative studies that integrate both the cutting force measurements and advanced 3D areal surface topography analysis under controlled experimental designs for this specific material and process combination.

While the primary focus of the present overview of existing studies is the effect of lubrication and cutting parameters on the forces and surface topography during high-feed face milling, it is important to also acknowledge the contribution of wiper-type inserts to

improvements in the surface integrity in milling and turning operations. Although wiper inserts are not the main subject of this research, their inclusion provides essential context for understanding the current surface finish enhancement strategies in high-feed machining. Wiper geometries are designed to extend the effective cutting edge, allowing a larger contact length with the workpiece and thereby smoothing the generated surface profile [44–46]. This design enables the combination of higher productivity with acceptable surface quality, which is directly relevant to the challenges addressed in this study. Several studies have demonstrated the advantages of wiper tools in both turning and milling. In the dry turning of laser-cladded parts [47], the use of wiper inserts significantly improved the material removal rate and surface finish compared with conventional inserts, although it also led to increased tool wear and the formation of built-up edges, potentially inducing tensile residual stresses on the machined surface. Similarly, in the hard machining of martensitic stainless steels using TiAlN-coated carbide tools [48], wiper edges enabled the maintenance of a fine surface quality and extended tool life even under dry conditions, confirming their suitability for high-efficiency applications. In milling, the development of a convex wiper edge on the rake face achieved up to a 35% improvement in surface finish across a wide feed range, allowing the same roughness quality at up to four times higher feed rates than conventional inserts [49]. Despite these benefits, the present study intentionally employed regular high-feed inserts to eliminate the additional surface-smoothing effect of wiper geometry, ensuring that the observed differences in surface quality and cutting force originate solely from the influence of lubrication and cutting parameters.

The present study addressed these gaps by conducting a systematic investigation of the high-feed face milling of medium carbon steel under dry and lubricated conditions. The study employed a controlled experimental setup using a single insert to simplify the analysis of cutting forces and isolate the effect of lubrication. Key parameters such as feed per tooth, cutting speed, and depth of cut were varied according to a DOE framework to evaluate their impact on machining performance. Cutting forces were measured with a three-component dynamometer, and the machined surface topography was analyzed using a 3D optical profiler. This integrated approach allows for the simultaneous evaluation of process mechanics and surface outcomes, enabling a comprehensive assessment of the lubrication effects, high-feed challenges, and optimal parameter selection. Ultimately, this study aims to provide understandings for the manufacturing industry by quantifying the effects of lubrication on the cutting forces, surface integrity, and process stability in high-feed milling. The research seeks to inform best practices for tool selection, process parameter optimization, and fluid application strategies. The findings will also serve as a foundation for further research into the interaction of tool geometry, lubrication, and cutting conditions in high-performance milling operations, bridging the gaps between experimental observation, industrial application, and theoretical understanding of machining mechanics.

2. Materials and Methods

To evaluate the influence of lubrication on the cutting forces and surface quality in the high-feed face milling of C45 steel, a series of cutting experiments were carried out under both dry and lubricated conditions. The methodology was developed to ensure a high degree of reproducibility and tribologically relevant observations.

The face milling operations were performed on a Perfect Jet MCV-M8 vertical machining center (Ping Jeng Machinery Industry, Taichung City, Taiwan). This CNC machining center offers the rigidity and precision necessary for cutting force investigations under high-feed conditions. The workpiece material selected for the study was C45 medium carbon steel, which is commonly used in general-purpose structural applications. The

machined area on each sample measured 50 mm in width and 40 mm in length, with a consistent flat surface ensured prior to each test.

To standardize the cutting conditions and isolate force effects, all experiments were performed using a single-insert configuration. A Tungaloy T2845 PM 063.05Z5W tool holder (Tungaloy Corporation, Iwaki, Fukushima, Japan) was used to mount a BFT Burzoni OFEX 05T3AE cutting insert (BFT Burzoni S.r.l., Podenzano, Italy). The insert was manufactured from KH100-grade carbide, optimized for milling operations involving medium carbon steels. The cutting edge geometry was selected to reflect a typical high-feed insert configuration. The major cutting edge angle was defined as $\kappa_r = 43°$, the orthogonal rake angle as $\gamma_o = 25°$, and the orthogonal flank angle as $\alpha_o = 7°$. The nose radius of the insert was $r_\varepsilon = 0.4$ mm, which provided a balance between cutting edge sharpness and edge strength. Using a single insert made it possible to directly correlate the cutting conditions with the three orthogonal force components, eliminating the influence of dynamic interactions between multiple edges. To ensure consistent cutting conditions throughout the experimental series, the condition of the cutting edge was regularly monitored. The insert was replaced whenever signs of micro-wear or degradation were observed, thereby minimizing the influence of edge wear on the surface integrity and force measurements.

The described setup (machine, workpiece, cutting tool) is shown in Figure 1.

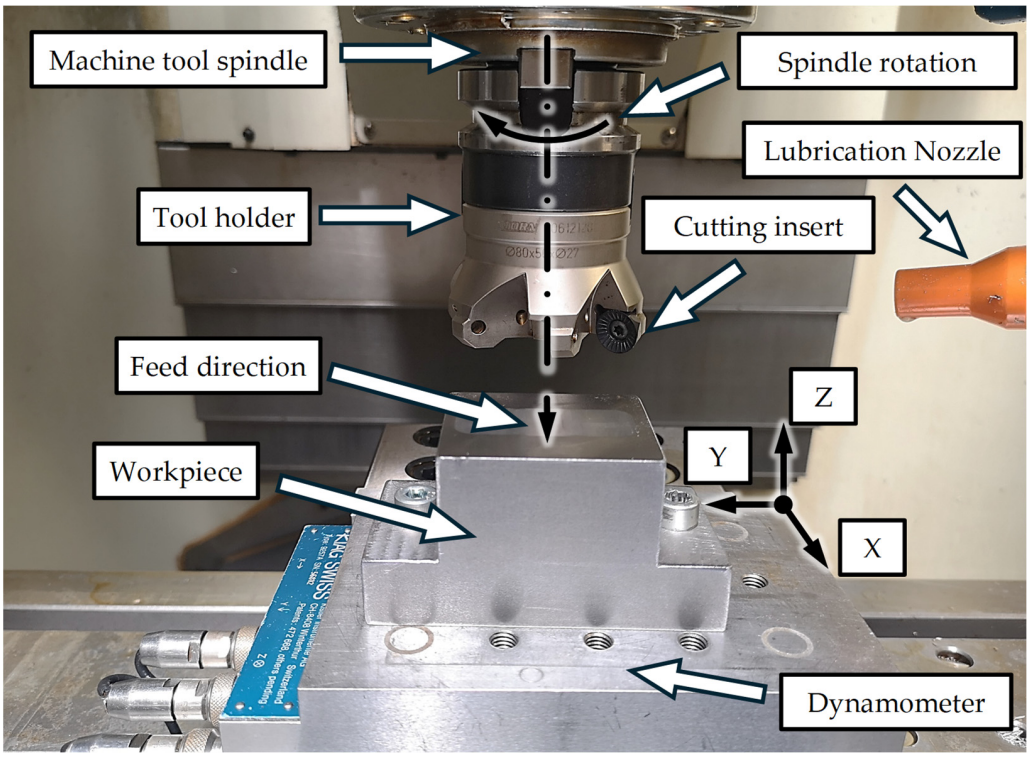


Figure 1. Experimental setup with the X (feed direction), Y (lateral direction), and Z (vertical direction) axes and kinematic relations.

Two lubrication conditions were evaluated: dry cutting with a flow rate of $Q = 0$ m^3/h, and wet cutting using a flooded cooling system delivering a 5% emulsion of Rhenus TS 25 coolant–lubricant at a flow rate of $Q = 2$ m^3/h. Rhenus TS 25 is an industrial-grade semi-synthetic emulsion formulated for enhanced cooling and lubricating properties in high-performance machining. The delivery of the fluid ensured complete coverage of the cutting zone and chip evacuation path, simulating a typical industrial flooded lubrication procedure. This design enabled a comparative assessment between the lubricated conditions and dry contact behavior.

A 2^4 full-factorial experimental design was employed to investigate the interactions between the primary cutting parameters and lubrication condition. Each setup was performed once. To validate repeatability, several randomly selected setups were repeated under identical conditions during the experiments. The results showed less than 5% deviation in cutting force components and less than 8% deviation in the surface roughness parameters, confirming high experimental consistency. Furthermore, each force signal was divided into multiple steady-state intervals to calculate the mean values, while the surface topography was evaluated using three independent, non-overlapping sub-areas for each measured region. This internal replication and cross-validation ensured that measurement dispersion remained within acceptable limits.

The experimental matrix included the following variables (Table 1): feed per tooth f_z = 0.8 mm/rev and f_z = 1.6 mm/rev, cutting speed v_c = 200 m/min and v_c = 400 m/min, depth of cut a_p = 0.3 mm and a_p = 0.6 mm, and lubrication flow rate Q = 0 m^3/h (dry) and Q = 2 m^3/h (wet). This design resulted in eight unique cutting setups, with all other parameters held constant. The selected ranges are representative of high-feed milling strategies used in industrial practice and allow for the analysis of both moderate and intensive material removal scenarios. The feed per tooth values reflect typical and increased feeds used in high-feed milling to maximize productivity. The cutting speeds were chosen to cover a range from conservative to high-performance conditions, with 400 m/min representing the upper limit of previous practice for C45 steel using coated carbide tools and effective cooling. The depths of cut were consistent with high-feed milling principles, where shallow depths are used to maintain low cutting forces per tooth and reduce tool deflection, especially under high feed rates. The lubrication flow rates represent dry and flood conditions, respectively, enabling a comparative analysis of the lubrication effects on the cutting forces and surface quality.

Table 1. Summary of the experimental setups.

Setup	f_z [mm/rev]	v_c [m/min]	a [mm]	Q [m^3/h]
1	0.8	200	0.3	0
2	1.6	200	0.3	0
3	0.8	400	0.3	0
4	1.6	400	0.3	0
5	0.8	200	0.6	0
6	1.6	200	0.6	0
7	0.8	400	0.6	0
8	1.6	400	0.6	0
9	0.8	200	0.3	2
10	1.6	200	0.3	2
11	0.8	400	0.3	2
12	1.6	400	0.3	2
13	0.8	200	0.6	2
14	1.6	200	0.6	2
15	0.8	400	0.6	2
16	1.6	400	0.6	2

Cutting forces were recorded using a Kistler 9257A three-component piezoelectric dynamometer (Kistler Instrumente AG, Winterthur, Switzerland) that was rigidly mounted beneath the workpiece. This system allows for the simultaneous acquisition of forces in the X (F_x), Y (F_y), and Z (F_z) directions, corresponding to the radial, feed, and axial directions, respectively. The dynamometer signals were conditioned through three Kistler 5011 (Kistler Instrumente AG, Winterthur, Switzerland) charge amplifiers, each assigned to one component of the force signal. These signals were subsequently digitized using an

NI-9215 analog input module, integrated into a NIcDAQ-9171 chassis (National Instruments (NI) Corporation, Austin, TX, USA). Force data acquisition was performed using NI LabVIEW 2018 SP1 (National Instruments (NI) Corporation, Austin, TX, USA). This setup provided high-resolution and low-noise force signals essential for cutting force decomposition and energy analysis. The sampling rate was set to 4000 Hz, which proved enough for the application.

After each milling experiment, the surface topography of the machined workpiece was characterized using an AltiSurf 520 three-dimensional topography measurement system (Altimet, Thonon-les-Bains, France). The scanning area was defined to fully cover the machined region and avoid transitional zones. The acquired topographical data were post-processed using AltiMap Premium 6.2.7487 software (Altimet, Thonon-les-Bains, France). Parameters were calculated in accordance with the ISO 25178 standard [50] to describe the tribologically relevant features of the machined surfaces. In the performed face milling experiments, the effects of cutting parameters—namely the cutting speed, axial depth of cut, and feed per tooth—as well as the application of cutting fluid were investigated in relation to the surface roughness characteristics of the machined surfaces. The evaluation included both profile (arithmetical mean height—R_a, root mean square deviation—R_q, maximum height of profile—R_z, maximum profile peak height—R_p, maximum profile valley depth—R_v, skewness—R_{sk}, kurtosis—R_{ku}) and areal (arithmetical mean height—S_a, root mean square deviation—S_q, maximum height—S_z, maximum peak height—S_p, maximum valley depth—S_v, skewness—S_{sk}, kurtosis—S_{ku}) surface roughness parameters. Care was taken to remove form and waviness components using leveling and filtering procedures. Among the studied roughness parameters, the skewness and kurtosis are less well-known, therefore their explanations are shown in Figure 2.

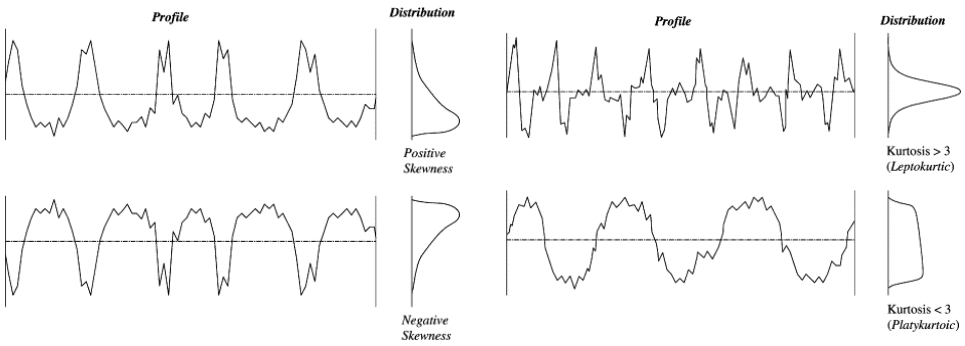


Figure 2. Clarification of the skewness and kurtosis of the surface [51].

3. Results

The cutting force and surface topography measurements were successfully conducted according to the experimental plan described in the previous section. All 16 machining configurations, derived from the full factorial design of experiments (DOE) approach, were performed under controlled laboratory conditions, ensuring repeatability and consistency across both dry and lubricated machining environments.

During the milling process, the three orthogonal components of the cutting force were measured using a piezoelectric dynamometer. In the coordinate system of the machine tool, the Y-direction corresponds to the principal cutting force component (F_c), which acts tangentially to the cutting edge and is responsible for material shearing. The Z-direction force (F_p), also referred to as the thrust force, is directed axially and reflects the vertical resistance against tool penetration. The X-direction force (F_f) acts along the feed direction. Due to the interrupted nature of face milling, the F_f component exhibits cyclic variations with alternating maximum and minimum values as the cutting edge enters and exits the

workpiece. Additionally, the resultant planar force (F_{xy}) was calculated from the X and Y components to characterize the total in-plane loading during machining. The force results for all 16 experimental setups are summarized in Table 2 including the maximum values of F_c, F_p, $F_{f,\max}$, $F_{f,\min}$, and the calculated F_{xy} for each configuration. Figure 3 illustrates the identification of characteristic cutting force extremes during high-feed face milling, using Setup 16 as an example to demonstrate the typical locations of the tangential (F_c), feed (F_f), and thrust (F_p) force maximum and minimum within one tool engagement cycle.

Table 2. Maximum values of the measured cutting forces.

Setup	$F_{c,max}$ [N]	$F_{f,max}$ [N]	$F_{f,min}$ [N]	$F_{xy,max}$ [N]	$F_{p,max}$ [N]
1	578.08	354.81	−285.44	580.24	436.07
2	942.06	565.95	−475.54	945.36	589.26
3	542.11	298.38	−239.58	544.14	446.03
4	915.66	474.83	−418.15	920.58	616.55
5	1030.08	650.40	−493.24	1036.22	667.76
6	1770.53	1043.5	−854.02	1776.02	876.42
7	967.31	538.16	−397.20	971.60	665.45
8	1712.38	855.76	−725.12	1719.52	886.04
9	572.53	355.51	−286.66	574.14	442.05
10	925.58	565.77	−475.08	928.05	583.48
11	543.57	295.41	−240.95	546.92	449.73
12	923.99	466.53	−398.40	928.27	609.35
13	1036.54	645.39	−488.84	1042.13	665.77
14	1714.66	1040.77	−850.36	1719.90	865.10
15	1011.75	537.14	−383.89	1019.60	692.58
16	1708.66	858.37	−686.98	1717.80	878.27

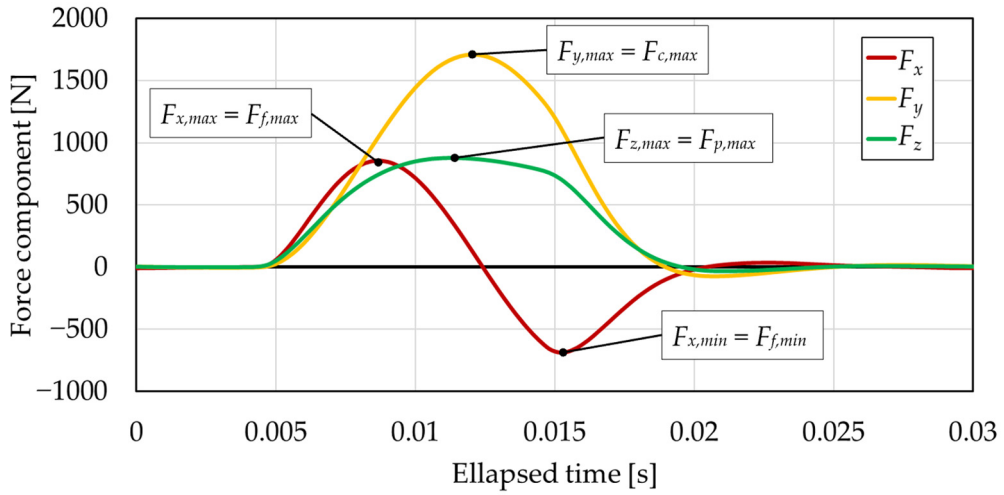


Figure 3. Identification of cutting force extremes in high-feed face milling (shown for Setup 16).

Following the machining process, the surface roughness of the milled workpiece areas was characterized using both 2D profile-based and 3D areal-based measurements. To illustrate the influence of feed rate on the surface texture, 3D surface topography maps were made for each setup. Figure 4 shows the surface obtained at a low feed rate (f_z = 0.8 mm/rev), while Figure 5 presents eight measurement positions captured at a high feed rate (f_z = 1.6 mm/rev). The 2D profile roughness parameters, including R_a, R_q, R_z, R_p, R_v, R_{sk}, and R_{ku}, are presented in Table 3. These parameters quantify the vertical deviation of surface features along a defined profile line. In parallel, 3D areal parameters such as S_a, S_q, S_z, S_p, S_v, S_{sk}, and S_{ku}, which offer a more comprehensive evaluation of surface texture over a defined area, are presented in Table 4. This dual characterization approach allows

for the cross-verification of results and a more complete interpretation of surface integrity under varying cutting conditions.

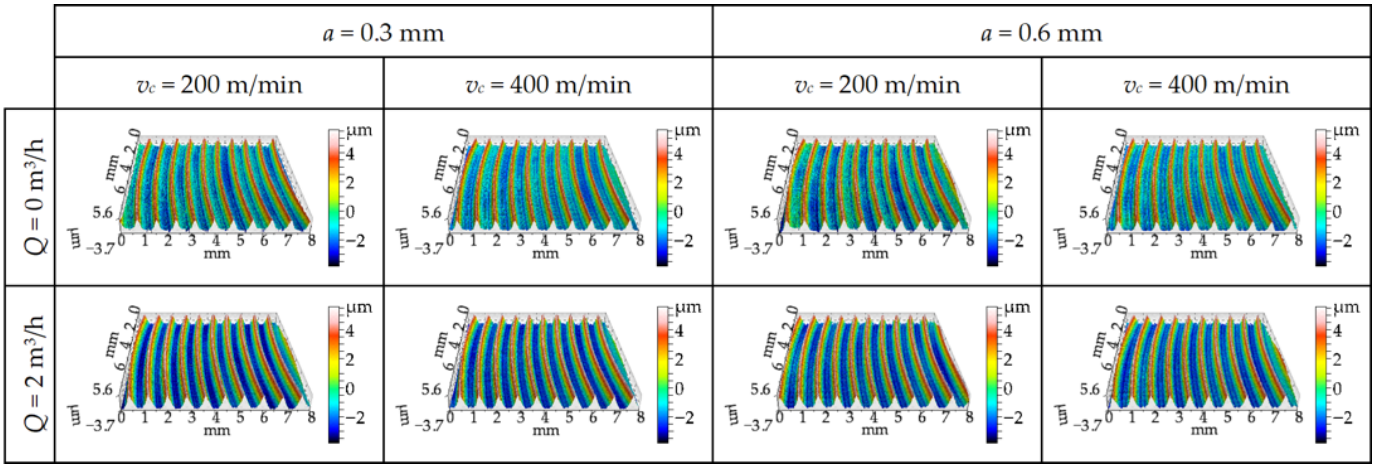


Figure 4. 3D surface topography of the milled surface at the low feed rate (f_z = 0.8 mm/rev).

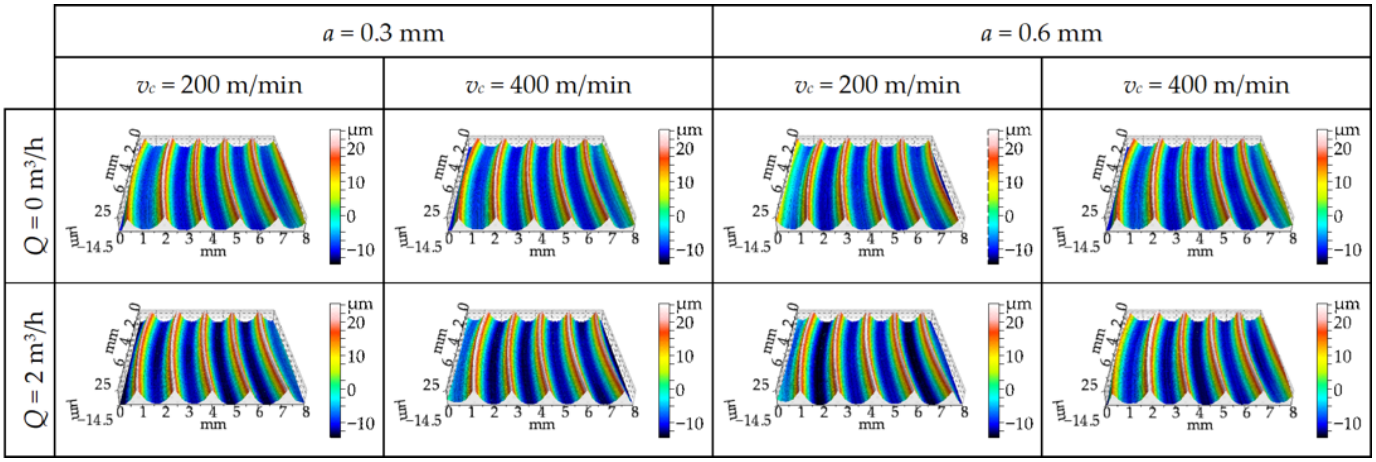


Figure 5. 3D surface topography of the milled surface at the high feed rate (f_z = 1.6 mm/rev).

Table 3. Measured 2D profile roughness parameters.

Setup	R_a [µm]	R_q [µm]	R_z [µm]	R_p [µm]	R_v [µm]	R_{sk} [-]	R_{ku} [-]
1	1.728	2.002	7.411	4.792	2.619	0.854	2.354
2	8.739	10.250	35.610	24.351	11.259	0.759	2.298
3	1.685	1.956	7.097	4.839	2.259	0.923	2.453
4	8.766	10.280	36.128	24.759	11.369	0.768	2.320
5	1.736	2.032	7.980	4.910	3.070	0.754	2.314
6	8.849	10.360	36.541	24.928	11.612	0.760	2.293
7	1.665	1.936	6.751	4.726	2.025	0.916	2.453
8	8.797	10.309	36.709	25.125	11.584	0.761	2.312
9	2.214	2.551	8.838	5.628	3.210	0.595	2.040
10	9.879	11.477	38.585	25.434	13.151	0.669	2.144
11	2.163	2.490	8.532	5.612	2.920	0.659	2.101
12	9.891	11.494	39.354	25.890	13.463	0.667	2.142
13	2.12	2.443	8.828	5.639	3.190	0.674	2.120
14	9.906	11.503	39.457	25.808	13.648	0.663	2.134
15	2.025	2.353	8.519	5.652	2.867	0.783	2.309
16	9.841	11.437	39.050	25.784	13.266	0.669	2.136

Table 4. Measured 3D areal roughness parameters.

Setup	S_a [µm]	S_q [µm]	S_z [µm]	S_p [µm]	S_v [µm]	S_{sk} [-]	S_{ku} [-]
1	1.719	2.029	8.852	5.173	3.680	0.854	2.484
2	8.768	10.342	36.116	24.527	11.590	0.813	2.396
3	1.668	1.956	7.608	5.132	2.475	1.001	2.616
4	8.834	10.405	36.632	24.680	11.953	0.793	2.364
5	1.762	2.094	9.720	5.434	4.286	0.785	2.445
6	8.963	10.532	36.909	24.775	12.134	0.798	2.359
7	1.628	1.923	7.719	5.088	2.631	0.991	2.636
8	8.847	10.424	37.062	24.861	12.201	0.802	2.379
9	2.227	2.566	9.450	5.914	3.535	0.605	2.050
10	9.985	11.636	40.397	26.132	14.265	0.699	2.196
11	2.200	2.538	9.211	5.838	3.373	0.688	2.143
12	10.001	11.647	39.212	26.017	13.195	0.723	2.212
13	2.152	2.486	9.744	6.015	3.729	0.690	2.156
14	10.000	11.659	39.728	26.113	13.615	0.725	2.222
15	2.087	2.424	9.093	5.885	3.207	0.771	2.282
16	9.938	11.582	39.222	25.989	13.233	0.7192	2.204

To capture the underlying trends and interactions between the machining parameters and measured responses, regression equations were derived based on the DOE methodology. These first-order equations with interaction terms model the effects of cutting speed, feed per tooth, depth of cut, and lubrication on the measured force components and surface roughness parameters. The developed models serve not only as predictive tools, but also as analytical instruments to identify dominant factors and their interaction effects. The resulting regression equations and their coefficients are detailed in the subsequent section.

The empirical models describing the variation of cutting force components and surface roughness parameters were determined using a full factorial experimental design. This method allowed for the evaluation of all combinations of the three main process parameters—cutting speed, feed per tooth, and lubrication condition—at two levels each. Based on the collected data, regression equations were formulated to quantify the individual and interaction effects of these parameters. Equations (1)–(12) present the fitted models corresponding to the experiments conducted with a constant axial depth of cut of 0.3 mm.

$$F_c\,(f_z,v_c,Q,a = 0.3) = 259.64 + 443.012{\cdot}f_z - 0.228{\cdot}v_c + 8.085{\cdot}Q + 0.06{\cdot}f_z{\cdot}v_c - 17.956{\cdot}f_z{\cdot}Q - 0.027{\cdot}v_c{\cdot}Q + 0.056{\cdot}f_z{\cdot}v_c{\cdot}Q \quad (1)$$

$$F_{f,max}\,(f_z,v_c,Q,a = 0.3) = 165.41 + 307.288{\cdot}f_z - 0.109{\cdot}v_c + 0.4{\cdot}Q - 0.217{\cdot}f_z{\cdot}v_c + 2.231{\cdot}f_z{\cdot}Q + 0.00195{\cdot}v_c{\cdot}Q - 0.014{\cdot}f_z{\cdot}v_c{\cdot}Q \quad (2)$$

$$F_{f,min}\,(f_z,v_c,Q,a = 0.3) = -129.67 - 252.038{\cdot}f_z + 0.172{\cdot}v_c + 8.345{\cdot}Q + 0.072{\cdot}fz{\cdot}vc - 11.1{\cdot}fz{\cdot}Q - 0.049{\cdot}v_c{\cdot}Q + 0.061{\cdot}f_z{\cdot}v_c{\cdot}Q \quad (3)$$

$$F_{xy}\,(f_z,v_c,Q,a = 0.3) = 262.54 + 442.25{\cdot}f_z - 0.237{\cdot}v_c + 6.175{\cdot}Q + 0.071{\cdot}f_z{\cdot}v_c - 17.081{\cdot}f_z{\cdot}Q - 0.018{\cdot}v_c{\cdot}Q + 0.05{\cdot}f_z{\cdot}v_c{\cdot}Q \quad (4)$$

$$F_p\,(f_z,v_c,Q,a = 0.3) = 290.25 + 169.82{\cdot}f_z - 0.037{\cdot}v_c + 10.44{\cdot}Q + 0.108{\cdot}f_z{\cdot}v_c - 7.888{\cdot}f_z{\cdot}Q - 0.00785{\cdot}v_c{\cdot}Q + 0.0026{\cdot}f_z{\cdot}v_c{\cdot}Q \quad (5)$$

$$S_a\,(f_z,v_c,Q,a = 0.3) = -5.17 + 8.675{\cdot}f_z - 0.0008{\cdot}v_c - 0.145{\cdot}Q + 0.00068{\cdot}f_z{\cdot}v_c + 0.48{\cdot}f_z{\cdot}Q + 0.00022{\cdot}v_c{\cdot}Q - 0.00021{\cdot}f_z{\cdot}v_c{\cdot}Q \quad (6)$$

$$S_q\,(f_z,v_c,Q,a = 0.3) = -6.07 + 10.213{\cdot}f_z - 0.0011{\cdot}v_c - 0.18{\cdot}Q + 0.00087{\cdot}f_z{\cdot}v_c + 0.53{\cdot}f_z{\cdot}Q + 0.00035{\cdot}v_c{\cdot}Q - 0.00031{\cdot}f_z{\cdot}v_c{\cdot}Q \quad (7)$$

$$S_z\,(f_z,v_c,Q,a = 0.3) = -15.43 + 31.9{\cdot}f_z - 0.015{\cdot}v_c - 3.39{\cdot}Q + 0.011{\cdot}f_z{\cdot}v_c + 3.988{\cdot}f_z{\cdot}Q + 0.00925{\cdot}v_c{\cdot}Q - 0.008438{\cdot}f_z{\cdot}v_c{\cdot}Q \quad (8)$$

$$S_p\,(f_z,v_c,Q,a = 0.3) = -13.96 + 23.962{\cdot}f_z - 0.00115{\cdot}v_c - 0.16{\cdot}Q + 0.0011{\cdot}f_z{\cdot}v_c + 0.68{\cdot}f_z{\cdot}Q + 0.0005{\cdot}v_c{\cdot}Q - 0.00071{\cdot}f_z{\cdot}v_c{\cdot}Q \quad (9)$$

$$S_v\,(f_z,v_c,Q,a = 0.3) = -1.47 + 7.938{\cdot}f_z - 0.014{\cdot}vc - 3.225{\cdot}Q + 0.00975{\cdot}f_z{\cdot}v_c + 3.3{\cdot}f_z{\cdot}Q + 0.008725{\cdot}v_c{\cdot}Q - 0.0076{\cdot}f_z{\cdot}v_c{\cdot}Q \quad (10)$$

$$S_{sk}\,(f_z,v_c,Q,a = 0.3) = 0.57 + 0.163{\cdot}f_z + 0.0016{\cdot}v_c - 0.095{\cdot}Q - 0.0011{\cdot}f_z{\cdot}v_c + 0.012{\cdot}f_z{\cdot}Q - 0.00045{\cdot}v_c{\cdot}Q + 0.00034{\cdot}f_z{\cdot}v_c{\cdot}Q \quad (11)$$

$$S_{ku}\,(f_z,v_c,Q,a = 0.3) = 2.24 + 0.125{\cdot}f_z + 0.0016{\cdot}v_c - 0.25{\cdot}Q - 0.0011{\cdot}f_z{\cdot}v_c + 0.081{\cdot}fz{\cdot}Q - 0.000375{\cdot}v_c{\cdot}Q + 0.00031{\cdot}f_z{\cdot}v_c{\cdot}Q \quad (12)$$

To further investigate the influence of increased cutting engagement, additional models were developed for the 0.6 mm depth of cut condition. The resulting Equations (13)–(24) represent these cases and allowed for a comparison with the lower depth of cut results. This separation facilitates a clearer understanding of the effect of axial depth on both the mechanical loading and surface generation mechanisms.

$$F_c\,(f_z,v_c,Q,a = 0.6) = 357.02 + 919.78{\cdot}f_z - 0.337{\cdot}v_c + 22.49{\cdot}Q + 0.029{\cdot}f_z{\cdot}v_c - 47.812{\cdot}f_z{\cdot}Q + 0.06{\cdot}v_c{\cdot}Q + 0.044{\cdot}f_z{\cdot}v_c{\cdot}Q \quad (13)$$

$$F_{f,max}\,(f_z,v_c,Q,a = 0.6) = 294.06 + 585.72\,f_z - 0.184{\cdot}v_c - 4.97{\cdot}Q - 0.47{\cdot}f_z{\cdot}v_c + 0.59{\cdot}f_z{\cdot}Q + 0.006625{\cdot}v_c{\cdot}Q + 0.0041{\cdot}f_z{\cdot}v_c{\cdot}Q \quad (14)$$

$$F_{f,min}\,(f_z,v_c,Q,a = 0.6) = 369.16 + 914.6\,f_z - 0.364{\cdot}v_c + 19.38{\cdot}Q + 0.051{\cdot}f_z{\cdot}v_c - 46.838{\cdot}f_z{\cdot}Q + 0.074{\cdot}v_c{\cdot}Q + 0.039{\cdot}f_z{\cdot}v_c{\cdot}Q \quad (15)$$

$$F_{xy}\,(f_z,v_c,Q,a = 0.6) = -195.64 - 492.05{\cdot}f_z + 0.316{\cdot}v_c + 10.9{\cdot}Q + 0.205{\cdot}f_z{\cdot}v_c - 16.444{\cdot}f_z{\cdot}Q - 0.042{\cdot}v_c{\cdot}Q + 0.08{\cdot}f_z{\cdot}v_c{\cdot}Q \quad (16)$$

$$F_p\,(f_z,v_c,Q,a = 0.6) = 473.34 + 245.913{\cdot}f_z - 0.071{\cdot}v_c - 23.675{\cdot}Q + 0.075{\cdot}f_z{\cdot}v_c + 10.15{\cdot}f_z{\cdot}Q + 0.137{\cdot}v_c{\cdot}Q + 0.008{\cdot}f_z{\cdot}v_c{\cdot}Q \quad (17)$$

$$S_a\,(f_z,v_c,Q,a = 0.6) = -5.29 + 8.97{\cdot}f_z - 0.00075{\cdot}v_c - 0.17{\cdot}Q + 0.00012{\cdot}f_z{\cdot}v_c + 0.41{\cdot}f_z{\cdot}Q + 0.00022{\cdot}v_c{\cdot}Q - 0.000062{\cdot}f_z{\cdot}v_c{\cdot}Q \quad (18)$$

$$S_q\,(f_z,v_c,Q,a = 0.6) = -6.12 + 10.475{\cdot}f_z - 0.0011{\cdot}v_c - 0.25{\cdot}Q + 0.00037{\cdot}f_z{\cdot}v_c + 0.5{\cdot}f_z{\cdot}Q + 0.000425{\cdot}v_c{\cdot}Q - 0.00021{\cdot}f_z{\cdot}v_c{\cdot}Q \quad (19)$$

$$S_z\,(f_z,v_c,Q,a = 0.6) = -13.32 + 31.3{\cdot}f_z - 0.021{\cdot}v_c - 3.07{\cdot}Q + 0.013{\cdot}f_z{\cdot}v_c + 3.006{\cdot}f_z{\cdot}Q + 0.0084{\cdot}v_c{\cdot}Q - 0.006281{\cdot}f_z{\cdot}v_c{\cdot}Q \quad (20)$$

$$S_p\,(f_z,v_c,Q,a = 0.6) = -13.16 + 23.663{\cdot}f_z - 0.038{\cdot}v_c - 0.38{\cdot}Q + 0.00262{\cdot}f_z{\cdot}v_c + 0.72{\cdot}f_z{\cdot}Q + 0.001155{\cdot}v_c{\cdot}Q - 0.0012{\cdot}f_z{\cdot}v_c{\cdot}Q \quad (21)$$

$$S_v\,(f_z,v_c,Q,a = 0.6) = -0.16 + 7.638{\cdot}f_z - 0.017{\cdot}v_c - 2.675{\cdot}Q + 0.011{\cdot}f_z{\cdot}v_c + 2.281{\cdot}f_z{\cdot}Q + 0.00685{\cdot}v_c{\cdot}Q - 0.005{\cdot}f_z{\cdot}v_c{\cdot}Q \quad (22)$$

$$S_{sk}\,(f_z,v_c,Q,a = 0.6) = 0.38 + 0.262{\cdot}f_z + 0.002{\cdot}v_c + 0.05{\cdot}Q + 0.00012{\cdot}f_z{\cdot}v_c + 0.005{\cdot}f_z{\cdot}Q + 0.00057{\cdot}v_c{\cdot}Q + 0.00034{\cdot}f_z{\cdot}v_c{\cdot}Q \quad (23)$$

$$S_{ku}\,(f_z,v_c,Q,a = 0.6) = 2.18 + 0.1{\cdot}fz + 0.0018{\cdot}vc - 0.25{\cdot}Q - 0.0011{\cdot}fz{\cdot}vc + 0.075{\cdot}fz{\cdot}Q - 0.00025{\cdot}vc{\cdot}Q + 0.000093{\cdot}f_z{\cdot}v_c{\cdot}Q \quad (24)$$

4. Discussion

This section provides an in-depth analysis of the experimental results regarding the cutting forces and surface topography under various high-feed face milling conditions. The influence of cutting parameters—cutting speed, feed per tooth, and axial depth of cut—along with the application of flood lubrication, was systematically examined. The findings are presented in two main categories: cutting force behavior and surface integrity, each further divided into key indicators.

4.1. Influence of Machining Parameters and Lubrication on Cutting Forces

This subsection evaluates the cutting force components recorded during the high-feed face milling of C45 steel. The tangential, feed, thrust, and resultant force values were examined individually and comparatively to assess the influence of the machining parameters and lubrication. Differences between dry and wet conditions were also highlighted to understand their effect on force generation and distribution.

During face milling with a radial immersion (width of cut) smaller than the tool diameter, the uncut chip thickness does not start from zero at edge entry nor fall to zero at exit. Instead, the cutting edge is always in partial engagement over a limited angular arc, so the local chip thickness varies between a finite minimum at the entry/exit extremes and a finite maximum somewhere within the contact arc. As the edge rotates through the engaged arc, the chip thickness increases from the entry minimum to a peak (when the engagement angle produces the largest chip cross-section) and then decreases back toward the exit minimum. This non-zero baseline of chip thickness in partial engagement explains why the force components never reach zero and why the in-cycle force waveform is asymmetric. The tangential force follows the overall chip-thickness envelope and therefore reached its maximum close to the location of the largest chip thickness, while the feed-directional force showed a positive peak during the early engagement and a negative

peak later in the cycle because of changes in the direction and magnitude of the cutting and ploughing components. The normal (thrust) force also tracks the chip load but is additionally modulated by contact length and tool geometry. Consequently, any change in feed per tooth or axial depth directly alters the peak and baseline chip thicknesses and thus produces proportional changes in the cutting force components, which explains the parameter sensitivities reported below.

4.1.1. Study of the Tangential Cutting Force Component

The tangential cutting force (F_c), corresponding to the Y-direction in the setup, represents the major cutting component during high-feed face milling. Figure 6 presents the variation of the tangential cutting force as a function of the cutting parameters, derived from the full factorial models given in Equations (1) and (13), corresponding to axial depths of cut of 0.3 mm and 0.6 mm, respectively.

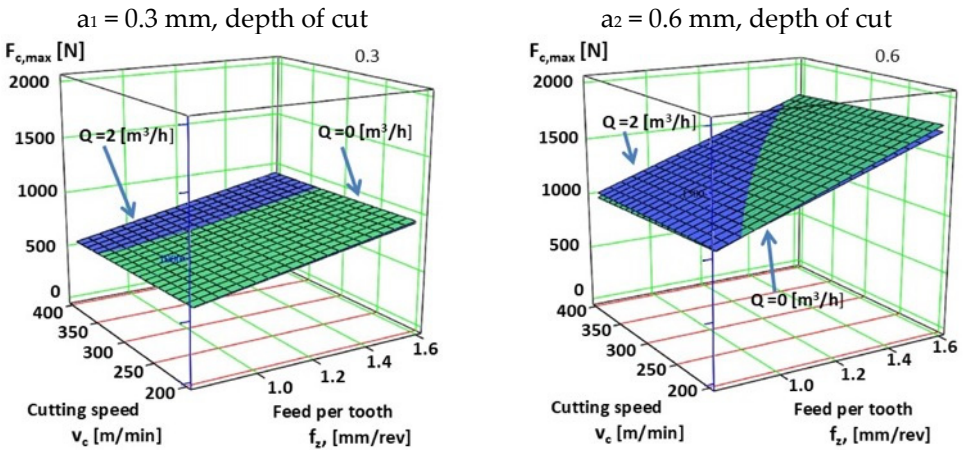


Figure 6. Alteration of the tangential cutting force.

The tangential cutting force was primarily affected by the feed per tooth, with depth of cut and cutting speed applying secondary effects. Increasing the feed from 0.8 to 1.6 mm/rev consistently produced significant rises in F_c across all conditions, confirming feed as the dominant factor due to greater chip thickness and material engagement. At a 0.3 mm depth and 200 m/min, F_c increased by about 63% under dry cutting, while similar proportional increases occurred at higher speeds and depths. The influence of depth of cut was nearly linear, with F_c approximately doubling as the depth increased from 0.3 to 0.6 mm, reflecting the direct relationship between engagement volume and cutting load. Cutting speed had a weaker yet discernible effect. At low feed, increasing the speed from 200 to 400 m/min slightly reduced the F_c (around 6–7%), attributed to thermal softening, which decreased the cutting resistance. However, at higher feeds and depths, this reduction became negligible, since the dominant influence of the increased chip load outweighed the temperature effects.

The effect of lubrication was marginal, typically within the range of 1–3%, which was close to the expected experimental variation. Such minor differences cannot be considered statistically significant but indicate a consistent trend of slightly lower forces under flood conditions. This suggests that lubrication primarily stabilizes the cutting process and may slightly smooth the force profile, rather than producing a measurable reduction in the mean tangential force.

In summary, F_c is primarily controlled by feed per tooth and depth of cut, with cutting speed and lubrication exerting secondary effects. High-feed and high-depth setups resulted in significantly higher tangential forces, and although flood lubrication slightly reduced the

F_c, its main effect lies in improving the cutting consistency and mitigating thermal loads rather than substantially lowering the peak force levels.

4.1.2. Assessment of the Maximum Feed Directional Force

The maximum feed force ($F_{f,max}$) corresponds to the positive peak in the X-direction, aligned with the feed motion of the tool. This force is critical for understanding the resistance encountered along the feed direction, influencing the material removal efficiency, tool deflection along the feed, and vibration susceptibility during high-feed milling. Figure 7 illustrates how the maximum value of the feed directional force changes in response to the applied cutting parameters, based on the predictive models defined by Equations (2) and (14) for the two investigated depths of cut.

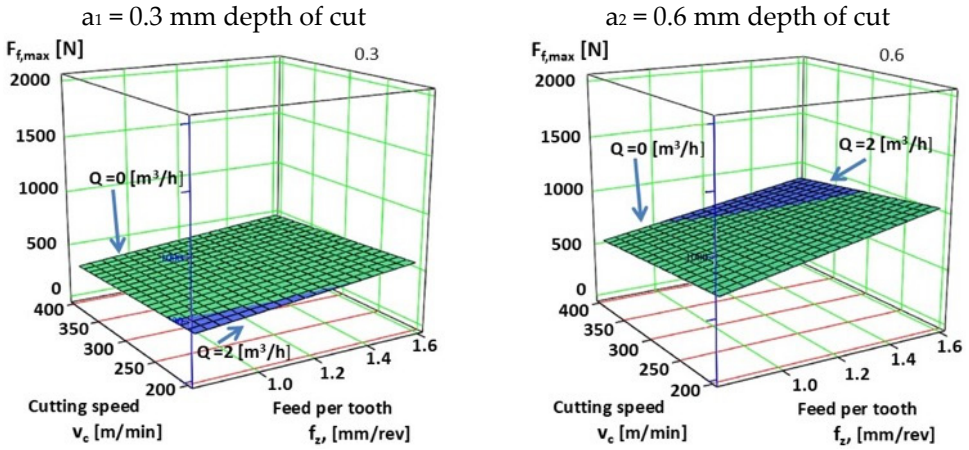


Figure 7. Alteration of the maximum value of the feed directional force.

Feed per tooth is the dominant factor influencing the maximum feed force in high-feed milling. Increasing the feed from 0.8 to 1.6 mm/rev caused the $F_{f,max}$ to rise by about 60% across all cutting speeds and depths, primarily due to the greater chip thickness and increased material engagement during tool entry. This relationship remained consistent regardless of depth, although higher depths of cut further amplified the effect, with forces nearly doubling when the depth increased from 0.3 to 0.6 mm. Cutting speed played a secondary role. At low feeds, increasing the speed from 200 to 400 m/min reduced the $F_{f,max}$ by around 15–16%, reflecting thermal softening of the workpiece and reduced cutting resistance. However, at higher feeds and depths, this effect weakened as the mechanical load from increased chip formation became the dominant influence. Depth of cut also contributed substantially, as a larger engagement volume intensifies the positive peak force generated early in the tool's engagement.

Lubrication showed only a marginal influence on $F_{f,max}$, with changes of around 1–3%, which lay within the expected measurement uncertainty. Although statistically minor, the trend toward slightly lower peaks suggests smoother tool–chip interaction under flooded conditions, possibly due to reduced local friction or improved chip evacuation rather than a measurable cooling effect. For example, at 0.8 mm/rev, 200 m/min, and 0.3 mm depth, the $F_{f,max}$ was 355 N in dry cutting and 356 N under flooded conditions, showing a minimal change due to the relatively small contribution of friction to this positive peak. At higher depths and feeds, lubrication slightly moderated $F_{f,max}$ by smoothing the friction spikes, which is particularly beneficial in reducing vibrations and promoting consistent tool motion.

Overall, $F_{f,max}$ was primarily influenced by the feed per tooth and depth of cut, with cutting speed and lubrication exerting secondary effects. Its peak value early in the engagement cycle reflects the instantaneous resistance of the workpiece along the

feed, while lubrication provides minor reductions and promotes smoother force evolution throughout the tool engagement. The analysis confirms that controlling the feed and depth is essential to manage positive feed forces, particularly under dry conditions where the friction and thermal effects are more pronounced.

4.1.3. Examination of the Minimum Feed Directional Force

The minimum feed force ($F_{f,min}$) represents the negative peak in the X-direction, occurring later in the cutting cycle, typically near the end of the third quarter of the tool engagement. This force provides insight into the tool–material interaction as the cutting edge exits the engagement zone and the chip geometry changes, influencing vibrations, chip flow, and residual stresses on the machined surface. Figure 8 portrays the influence of cutting parameters on the minimum value of the feed directional force, calculated using the regression models provided in Equations (3) and (15) for the respective depths of cut.

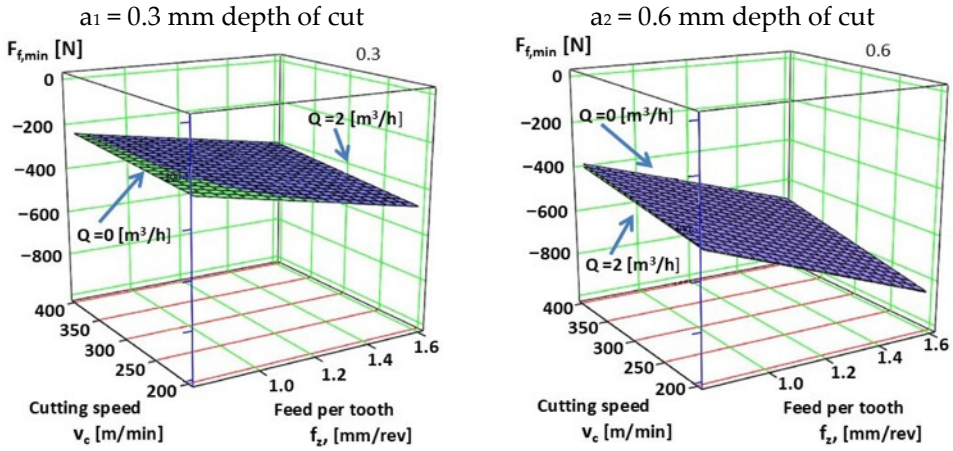


Figure 8. Alteration of the minimum value of the feed directional force.

Feed per tooth had the most significant influence on the minimum feed force. Increasing the feed from 0.8 to 1.6 mm/rev consistently intensified the negative peak, with the magnitude rising by about 65–75% across all speeds and depths. This behavior reflects the greater chip thickness and material resistance encountered as the cutting edge exits the workpiece during the latter phase of engagement. Cutting speed showed a secondary effect. Raising the speed from 200 to 400 m/min slightly reduced the magnitude of $F_{f,min}$, particularly at lower feeds, due to thermal softening of the workpiece and reduced frictional resistance. The reduction was modest—typically around 15–16%—and became negligible at higher feed or depth levels, where geometric and material engagement effects dominate. Depth of cut further amplified the negative feed force. When the depth doubled from 0.3 to 0.6 mm, $F_{f,min}$ increased by roughly 70–80% across most cutting conditions, underscoring the strong influence of engagement volume on exit-stage resistance.

Flood lubrication produced only minor differences in $F_{f,min}$, typically between 1% and 4%, which remained within the uncertainty of the experimental data. However, the results consistently showed a directionally stable trend toward slightly smoother force signals under lubrication, implying a reduction in frictional fluctuations rather than a real decrease in mean force magnitude. For example, at 0.8 mm/rev, 200 m/min, and 0.3 mm depth, $F_{f,min}$ changed from −285 N (dry) to −287 N (flooded), a negligible effect for low feeds but slightly more noticeable at higher feeds and depths. Flood lubrication smoothed the frictional spikes and reduced the thermal stresses, contributing to a more stable force profile during the latter portion of the tool engagement. This is particularly important for high-feed milling, where vibrations induced by the negative feed peak can affect the surface finish and dimensional accuracy.

In summary, $F_{f,min}$ was dominated by feed per tooth and depth of cut, reflecting the material resistance encountered at the final stages of tool engagement. Cutting speed had a minor reducing effect, and lubrication slightly stabilized the negative peak. Understanding the behavior of $F_{f,min}$ is crucial for minimizing tool vibrations, maintaining surface quality, and ensuring consistent chip flow in high-feed milling operations, particularly under dry conditions where the friction and thermal effects are more pronounced.

4.1.4. Integrated Evaluation of Feed Force Extremes

The feed forces in high-feed milling, represented by $F_{f,max}$ and $F_{f,min}$, describe the dynamic resistance along the feed direction during tool engagement. $F_{f,max}$ occurred early in the cutting cycle, near the end of the first quarter of tool engagement, reflecting the initial resistance as the cutting edge engages the workpiece. $F_{f,min}$ appeared later, near the end of the third quarter, representing the resistance as the tool exits the engagement zone. The difference between these two peaks indicates the total force fluctuation along the feed direction, providing insights into the vibration potential, tool deflection, and surface quality.

Both the maximum and minimum feed directional forces were primarily affected by feed per tooth, with depth of cut applying a strong secondary influence. As the feed increased from 0.8 to 1.6 mm/rev, both peaks rose markedly across all conditions. The positive peak ($F_{f,max}$), occurring during the initial tool engagement, grew by roughly 55–60%, while the negative peak ($F_{f,min}$), associated with tool exit, increased by 65–75%. This reflects the larger chip thickness and greater material resistance encountered at higher feeds, which heighten the force variation throughout the cutting cycle. The combined effect of these changes is a substantial widening of the force range. At 0.3 mm depth and 200 m/min, the alternation between $F_{f,max}$ and $F_{f,min}$ increased from about 640 N at 0.8 mm/rev to over 1000 N at 1.6 mm/rev. Similar trends were observed at higher speeds and depths, confirming that feed per tooth not only raises individual peaks but also amplifies the total fluctuation in feed force. This wider force range can increase the tool deflection and vibration potential, influencing dimensional accuracy and surface finish in high-feed milling. Cutting speed had a more limited effect. Increasing it from 200 to 400 m/min slightly lowered both $F_{f,max}$ and $F_{f,min}$—typically by 10–15% at lower feeds—due to mild thermal softening and reduced friction. However, this smoothing effect diminished at higher feeds and depths, where material engagement dominates. Depth of cut, conversely, exerted a pronounced effect on both peaks. Doubling the depth from 0.3 to 0.6 mm could raise the $F_{f,max}$ by about 80–90% and increase the $F_{f,min}$ in magnitude by 70–80%, leading to significantly higher total oscillation amplitudes.

Flood lubrication had a negligible quantitative effect on the feed forces (within $\pm$3%) but provided a qualitatively smoother force response. Although the absolute reduction was statistically insignificant, the consistent narrowing of the force range suggests that lubrication may improve the chip formation and tool engagement rather than materially lowering the load. Under flooded conditions, $F_{f,max}$ slightly decreased in most setups. For instance, at 0.8 mm/rev, 200 m/min, and 0.3 mm depth, $F_{f,max}$ was 355 N dry and 356 N flooded, showing negligible change at low feed. At higher feeds and depths, lubrication slightly reduced the peaks and smoothed the force profile. Ff min exhibited a similar trend, with minor reductions in magnitude.

The combined analysis of $F_{f,max}$ and $F_{f,min}$ shows that feed per tooth and depth of cut dominated both the individual peaks and the total oscillation of feed forces. Cutting speed slightly mitigated the peaks at low feed and depth but had little impact under extreme cutting conditions. Flood lubrication provided minor reductions in peak values and narrowed the range of oscillation, contributing to smoother force profiles and more

stable milling conditions. Understanding both the peaks and dynamic range is critical for process planning in the high-feed milling of medium carbon steels, particularly to minimize vibrations, ensure dimensional accuracy, and maintain surface integrity.

4.1.5. Analysis of the Resultant Force in the Machined Plane

The resultant force F_{xy}, calculated as the vector sum of F_x and F_y, represents the total force acting in the machined surface plane. It provides a comprehensive view of the combined effect of tangential and feed forces, reflecting the overall load the tool experiences during cutting. The analysis of F_{xy} is essential for understanding the tool deflection, vibration potential, and surface quality in high-feed milling operations. As illustrated in Figure 9, the behavior of the resultant force within the machined surface plane showed a distinct pattern, which can be interpreted based on the formulations provided in Equations (4) and (16).

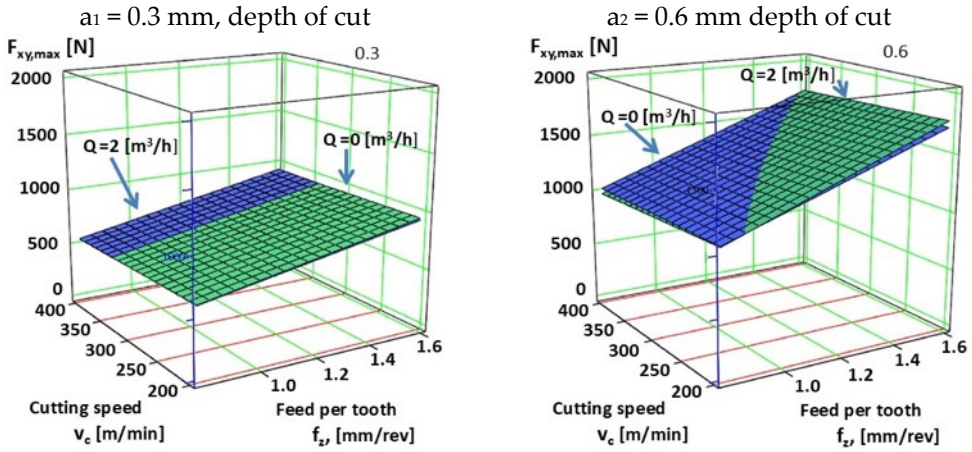


Figure 9. Alteration of the resultant force in the machined surface plane.

Feed per tooth was the most influential factor affecting the resultant in-plane force. Increasing the feed from 0.8 to 1.6 mm/rev significantly raised F_{xy} across all cutting speeds and depths. At 0.3 mm depth and 200 m/min, F_{xy} rose from 580 N to 945 N (about 63%), while at 400 m/min, the increase was from 544 N to 921 N (around 69%). At a deeper cut of 0.6 mm, the same feed increase raised the F_{xy} from 1036 N to 1776 N (about 71%) at 200 m/min, and from 972 N to 1720 N (roughly 77%) at 400 m/min. These results confirm that higher feeds intensify both the tangential and feed force components, producing a considerably larger resultant load on the tool. Depth of cut also applied a strong effect. Doubling it from 0.3 to 0.6 mm increased F_{xy} by approximately 70–80% under all feed and speed combinations due to greater material engagement and higher total cutting resistance. For instance, at 0.8 mm/rev and 200 m/min, F_{xy} increased from 580 N to 1036 N, while at 1.6 mm/rev, it grew from 945 N to 1776 N. Cutting speed showed only a moderate influence. Raising it from 200 to 400 m/min slightly reduced the F_{xy}—typically by 5–7%—at lower feeds, reflecting the reduced friction and mild thermal softening. However, at higher feeds and depths, this effect became negligible, as the dominant determinants of F_{xy} remained the feed per tooth and depth of cut, which jointly govern tool loading and chip formation uniformity.

The influence of lubrication on F_{xy} was minimal, with changes of around 1–3%, generally within the statistical scatter of the data. Although these small reductions were not significant in magnitude, the consistency of the trend implies that lubrication marginally stabilizes the resultant force through improved chip evacuation and friction smoothing rather than through direct cooling. For example, at 0.8 mm/rev, 200 m/min, and 0.3 mm depth, F_{xy} was 580 N under dry cutting and 574 N under flooded conditions. Although

the reduction was minor, it was consistent across conditions, suggesting that lubrication helps in smoothing force fluctuations and mitigating the potential for chatter and vibration, particularly in high-feed operations. The combined effect of feed, depth, cutting speed, and lubrication on F_{xy} illustrates the interplay between process parameters. Feed and depth were the primary factors controlling the magnitude of the resultant force, while cutting speed and lubrication provided secondary stabilization and slight reductions. High F_{xy} values corresponded to setups with high feed and deep cuts, which require robust tool support and machine rigidity. Flood lubrication, even with small reductions in force magnitude, contributed to more consistent tool–workpiece interaction and steadier chip evacuation, thereby reducing the likelihood of surface irregularities and improving process reliability.

In conclusion, F_{xy} integrates the contributions of tangential and feed forces, providing a clear picture of the total load acting in the machined surface plane. Feed per tooth and depth of cut dominated the resultant force, while speed and lubrication influenced it moderately. Monitoring and controlling F_{xy} are crucial for the high-feed milling of medium carbon steels, particularly to maintain surface quality and prevent excessive deflection or vibration, with flood lubrication providing additional support for consistent and reliable machining outcomes.

4.1.6. Evaluation of the Thrust Force Acting Normal to the Surface

The thrust force, F_p, acting in the Z-direction perpendicular to the machined surface, plays a critical role in determining tool deflection, workpiece distortion, and overall process stability. Analysis of the experimental dataset revealed clear trends with respect to feed per tooth, cutting speed, depth of cut, and lubrication. Figure 10 illustrates the changes in thrust force observed during machining, as derived from the analytical basis provided by Equations (5) and (17).

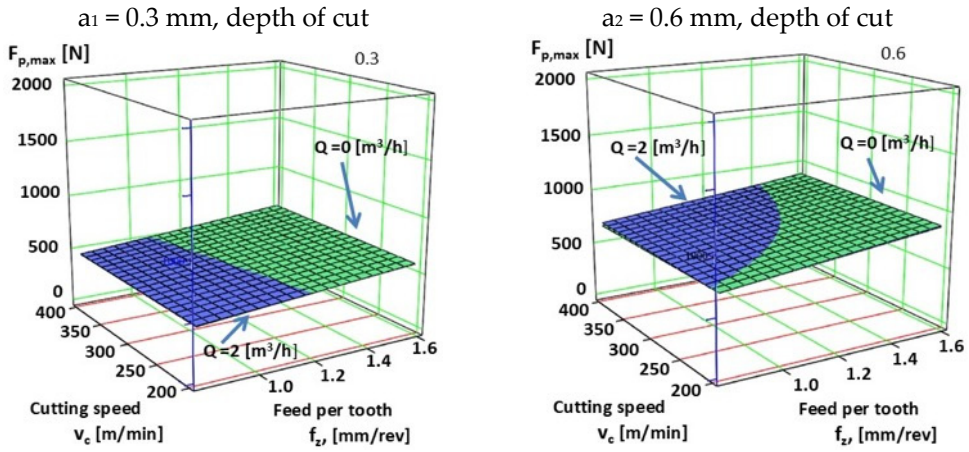


Figure 10. Alteration of the thrust force.

Feed per tooth had the most significant impact on the thrust force (F_p). Increasing the feed from 0.8 to 1.6 mm/rev consistently raised F_p across all cutting conditions. At 0.3 mm depth and 200 m/min under dry cutting, F_p rose from about 436 N to 589 N—an increase of roughly 35%. At 400 m/min, the same feed change raised the F_p from 446 N to 617 N (around 38%). This effect became stronger at greater depths of cut: at 0.6 mm depth, F_p increases from 668 N to 876 N at 200 m/min, and from 665 N to 886 N at 400 m/min, corresponding to increases of 31–33%. These results confirm that feed per tooth affects the normal load acting on the tool, as higher feeds generate thicker chips and stronger perpendicular forces. Cutting speed had a comparatively minor influence. When the speed was raised from 200 to 400 m/min, the F_p changed only slightly—by about 2–4%—depending on the feed and depth. At low feed (0.8 mm/rev), F_p increased

marginally from 436 N to 446 N, while at higher feed (1.6 mm/rev) and 0.6 mm depth, it rose from 876 N to 886 N. This indicates that thermal softening has a limited effect under high-feed conditions, where material engagement dominates. Depth of cut exhibited a nearly linear relationship with F_p. Doubling the depth from 0.3 mm to 0.6 mm increased F_p by about 50%, both at low and high feeds, emphasizing its role in enhancing the normal cutting resistance. Consequently, depth and feed together largely determine the F_p magnitude and potential for tool deflection or part deformation during high-feed milling.

Flood lubrication showed a minor and statistically insignificant influence on F_p, typically 1–4% lower on average. These small variations indicate that lubrication did not meaningfully alter the mean normal load but may have reduced transient force fluctuations by lowering the interfacial friction and improving chip evacuation. For example, at 0.8 mm/rev, 200 m/min, and 0.3 mm depth, F_p decreased from 436 N (dry) to 442 N (flooded). The effect was more notable in high-feed and higher-depth conditions, where lubrication helped in reducing the peak thermal stresses and preventing sudden increases in F_p due to material adhesion or friction spikes.

Overall, the thrust force was primarily influenced by feed per tooth and depth of cut, reflecting the combined effect of chip thickness and normal cutting resistance. Cutting speed had a secondary influence, and lubrication contributed to force stabilization rather than dramatic reductions. The magnitude of F_p in high-feed and high-depth setups was substantial, emphasizing the need for careful tool support and machine rigidity, particularly when dry conditions are employed. The application of flood lubrication, despite only moderate reductions in F_p, reduced the risk of force-induced tool deflection or premature wear, supporting a more repeatable and predictable cutting process.

4.2. Influence of Machining Parameters and Lubrication on Surface Topography

This subsection discusses the measured surface topography parameters from both the profile and areal roughness perspectives. The analysis investigated how different machining setups and lubrication conditions influence surface texture features such as height amplitude, distribution symmetry, and peak characteristics. The results provide insights into the relationship between the cutting dynamics and surface integrity.

Figures 4 and 5 present the three-dimensional surface textures obtained after high-feed face milling under various cutting parameters and lubrication conditions. The surfaces clearly revealed the distinct geometric marks of the tool paths, where each feed mark corresponded to an individual insert engagement. At the lower feed (Figure 4), the surface exhibited relatively shallow feed marks and smooth wave-like patterns, particularly at lower depths of cut (a = 0.3 mm). The overlap between successive tool paths was significant, resulting in a more continuous surface with smaller height variations. Increasing the depth of cut to a = 0.6 mm slightly intensified the amplitude of the marks but preserved the uniform periodicity. The application of flood lubrication reduced minor surface irregularities and produced more uniform grooves, which appeared less fragmented compared with dry cutting. The surface under v_c = 400 m/min showed slightly more regular feed traces, suggesting improved chip evacuation and reduced adhesion effects at higher speeds. In contrast, at the higher feed rate (Figure 5), the topographies became markedly more pronounced, with deeper feed marks and higher peak-to-valley distances. The periodic pattern was more distinct, and the ridge crests were clearly separated, indicating a coarser texture dominated by kinematic effects. Under dry conditions, localized irregularities and sharper peak transitions could be observed, while under flooded lubrication, the groove geometry remained well-defined but appeared cleaner and less interrupted by a probable built-up edge formation. Increasing the cutting speed produced a small smoothing of the surface peaks, especially at a = 0.3 mm, suggesting a reduction in adhesion-related defects.

Overall, these surface plots visually demonstrate the combined influence of feed rate, depth of cut, and lubrication on the geometric texture formation during high-feed milling.

4.2.1. Evaluation of Selected Roughness Amplitude Parameters

The arithmetical mean height (R_a, S_a) and root mean square roughness (R_q, S_q) provide essential insight into the average and statistical deviation of the surface profile and area. These parameters are sensitive to tool engagement, chip formation mechanics, and thermal effects. Figure 11 demonstrates how the arithmetical mean height varied across the machined surface, as established through Equations (6) and (18), while Figure 12 presents the corresponding changes in root mean square roughness, derived from Equations (7) and (19).

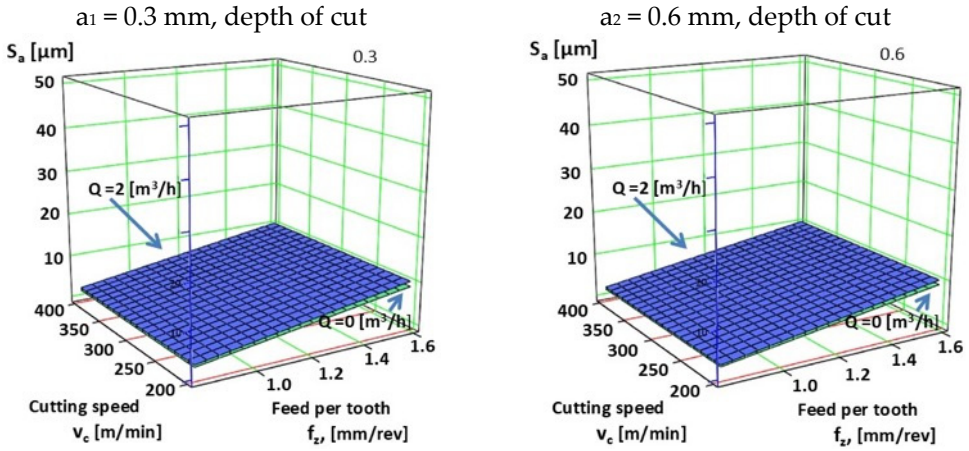


Figure 11. Alteration of the arithmetical mean height.

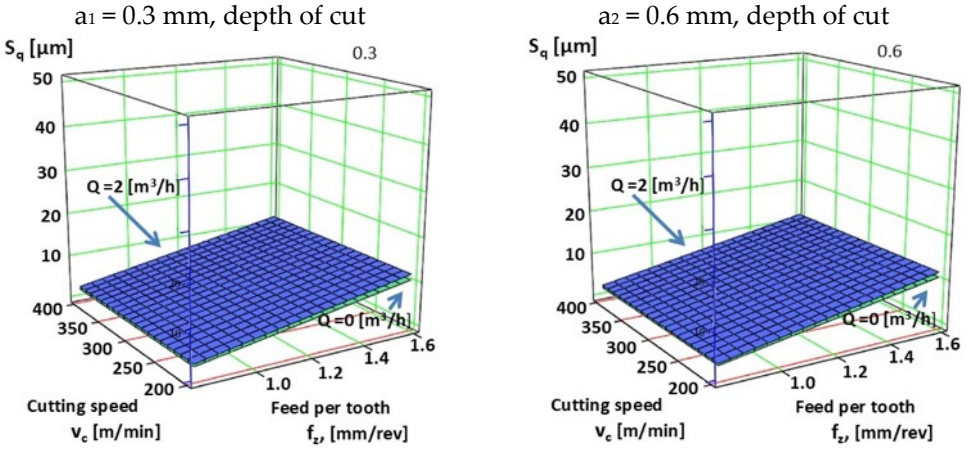


Figure 12. Alteration of the root mean square roughness.

Feed per tooth was the dominant factor affecting the average roughness parameters. Under dry conditions, increasing the feed from 0.8 to 1.6 mm/rev caused R_a to rise from about 1.7 µm to 8.8 µm and S_a from 1.7 µm to 8.9 µm—over a fivefold increase. R_q and S_q followed similar trends, reaching roughly 10.5 µm at the highest feed. This strong effect was attributed to the larger uncut chip thickness, which deepens feed marks and enhances surface irregularities. On average, the increase in roughness exceeded 400%, confirming that higher feed rates significantly deteriorate both the profile and areal surface quality. Cutting speed had a weaker influence but still produced slight improvements at lower feeds. When the speed increased from 200 to 400 m/min, R_a and S_a decreased modestly (from 1.728 to 1.685 µm and from 1.719 to 1.668 µm, respectively), representing a 2–4%

reduction. R_q and S_q showed similar minor declines, suggesting smoother cutting marks at higher speeds due to reduced friction and vibration. However, at high feeds, this effect was negligible (<1%). Depth of cut also affected the surface quality but to a lesser extent. At 0.8 mm/rev and 200 m/min, increasing the depth from 0.3 to 0.6 mm raised the R_a and S_a by only about 2–3%. Under high feed, the increase reached roughly 2%. These results confirm that while feed dominates roughness formation, depth and speed exert secondary, interactive effects.

The application of flood lubrication had a stabilizing but relatively moderate effect. Across all configurations, lubricated conditions yielded roughness values 2–6% higher than dry setups at the lowest feeds and 1–3% lower at the highest feeds. For example, at 0.8 mm/rev, 200 m/min, and 0.3 mm depth, R_a increased from 1.728 µm (dry) to 2.214 µm (wet), while at 1.6 mm/rev, 400 m/min, and 0.6 mm depth, R_a changed slightly from 8.797 µm (dry) to 9.841 µm (wet). In most cases, the differences in R_a, S_a, R_q, and S_q between dry and wet machining were within ±6%.

In general, the results confirm that a higher feed per tooth dominates roughness formation, cutting speed has a secondary smoothing effect, depth of cut causes modest increases, and lubrication tends to dampen extreme values but does not reverse the effect of aggressive feed or depth.

4.2.2. Investigation of Peak and Valley Height Metrics

The roughness parameters R_z, R_p, R_v (profile-based) and S_z, S_p, S_v (areal-based) provide critical insights into the peak-to-valley characteristics of the machined surface. These values are particularly relevant when evaluating functional surface properties such as contact mechanics, lubrication retention, and fatigue resistance. In this study, the effects of feed per tooth, cutting speed, depth of cut, and lubrication application were systematically investigated for their impact on these extreme amplitude parameters. Figure 13 displays the variation in maximum height across the machined surface, as calculated using Equations (8) and (20). The changes in maximum peak height are illustrated in Figure 14, based on the analytical expressions provided in Equations (9) and (21). Figure 15 shows the maximum valley depth, derived from the relationships defined in Equations (10) and (22).

Feed per tooth was again the most dominant factor influencing the extreme height parameters. Under dry conditions, doubling the feed from 0.8 to 1.6 mm/rev caused large increases across all six parameters. R_z rose from 7.41 µm to 35.61 µm (≈380%), and S_z from 8.85 µm to 36.12 µm (≈310%). Similarly, R_p and S_p increased by about 370%, while R_v and S_v rose by more than 400%. These pronounced changes show that higher feed rates deepen both peaks and valleys, consistent with greater uncut chip thickness and intensified tool–workpiece interaction. Cutting speed had a secondary, slightly improving effect on low feeds. When increased from 200 to 400 m/min at 0.8 mm/rev, R_z decreased from 7.41 µm to 7.10 µm (≈4%) and S_z from 8.85 µm to 7.61 µm (≈14%), indicating smoother surfaces at higher speeds. However, at 1.6 mm/rev, this effect became negligible, with most parameters changing by less than 1%. Depth of cut had a smaller but still noticeable influence. At 0.8 mm/rev and 200 m/min, increasing the depth from 0.3 to 0.6 mm raised R_z by about 8% and S_z by about 10%. Under high-feed conditions, increases were limited. Valley parameters (R_v and S_v) tended to rise slightly more than peaks, suggesting that larger depths enhance valley formation due to stronger tool engagement and chip flow interactions.

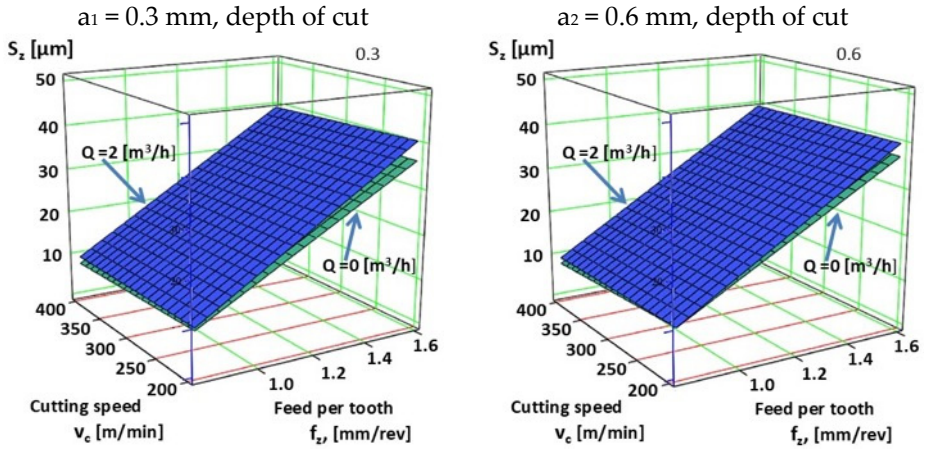


Figure 13. Alteration of the maximum height.

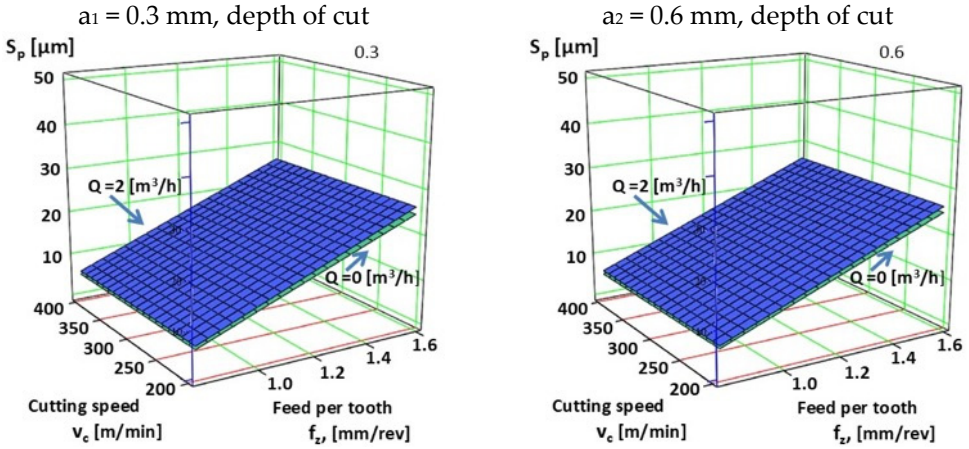


Figure 14. Alteration of the maximum peak height.

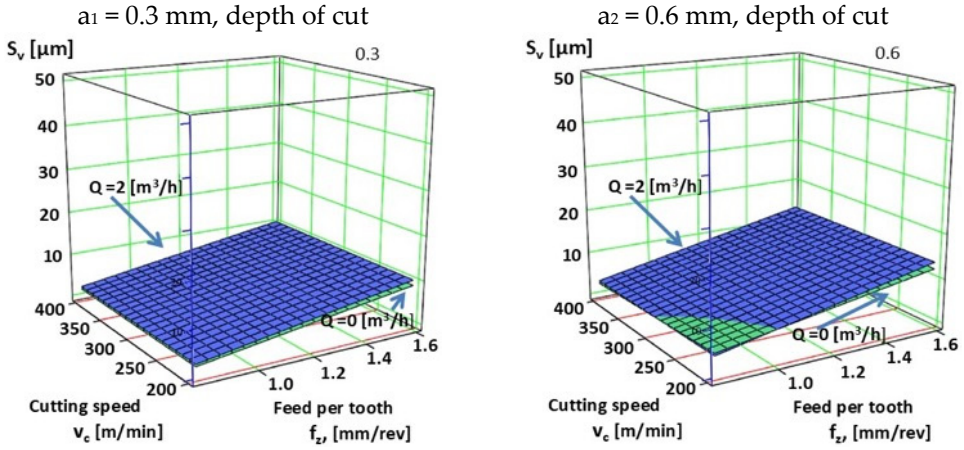


Figure 15. Alteration of the maximum valley depth.

The use of flood lubrication slightly altered the extreme roughness profile. At 0.8 mm/rev, the application of coolant increased R_z from 7.41 µm to 8.84 µm (~19.2%) and S_z from 8.85 µm to 9.45 µm (~6.8%). However, at higher feeds, lubrication contributed to a moderate rise in peak and valley extremes: R_z values rose from 35.61 µm (dry) to 38.59 µm (wet), and S_z from 36.12 µm to 40.39 µm. While this may initially seem unfavorable, the increased height parameters under wet conditions can be attributed to improved chip evacuation and reduced built-up edge, which alter the material removal mechanism and produce a more varied microtopography. The average increases for R_p and S_p across all

wet conditions ranged between 2% and 9%, while R_v and S_v saw higher increases of up to 22%, especially at high feed and depth combinations. Interestingly, under dry machining, the valleys (R_v, S_v) were generally shallower than under wet conditions, possibly due to thermal softening and smearing effects. Lubrication prevented such effects and facilitated sharper material removal, resulting in deeper but cleaner valleys.

In summary, feed per tooth had the most significant impact, followed by depth of cut, while cutting speed played a minor smoothing role. Flood lubrication tended to amplify the extremes slightly but resulted in more controlled and predictable surface formation, especially in high-feed regimes.

4.2.3. Study of Height Distribution Shape Parameters

Skewness (R_{sk} and S_{sk}) and kurtosis (R_{ku} and S_{ku}) offer insight into the statistical distribution and symmetry of surface heights. These parameters, although less commonly emphasized than amplitude descriptors, are crucial in tribological contexts, as they influence lubrication retention, contact area behavior, and the initiation of wear. In this study, the skewness and kurtosis values were analyzed to understand how machining parameters and lubrication application affected the texture profile distribution during the high-feed face milling of C45 steel. Figure 16 illustrates the variation in surface skewness, as determined from the analytical expressions in Equations (11) and (23). The changes in kurtosis are presented in Figure 17, based on the modeling approach defined by Equations (12) and (24).

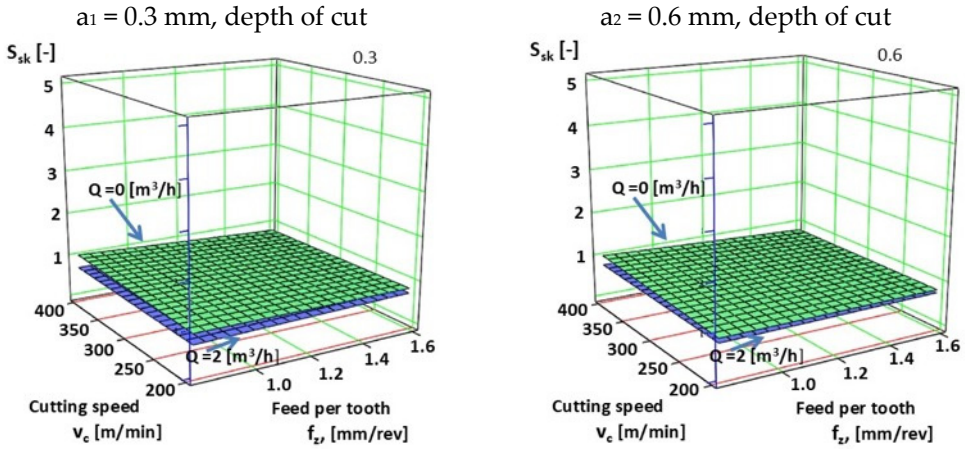


Figure 16. Alteration of the skewness.

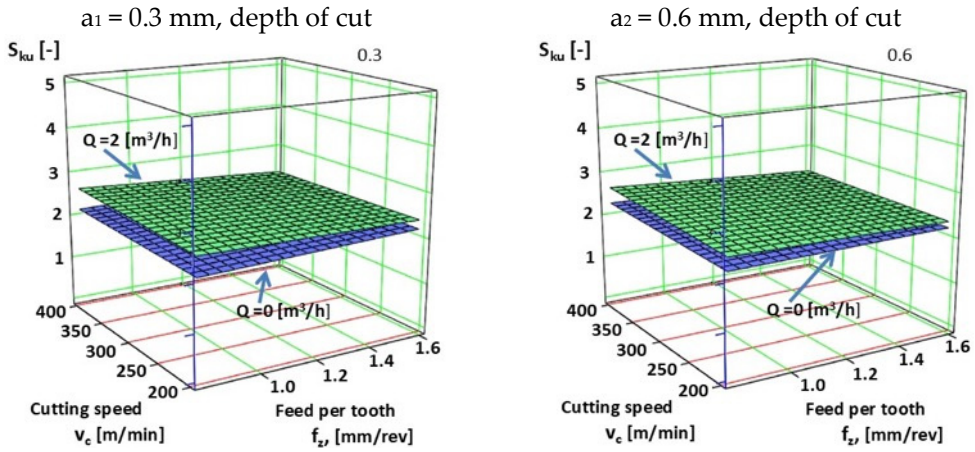


Figure 17. Alteration of the kurtosis.

The R_{sk} and S_{sk} parameters, indicating surface asymmetry, remained positive across all setups, reflecting peak-dominated textures typical of milled surfaces. Under dry conditions,

values ranged from 0.75 to 1.00, with slightly lower skewness observed at higher depths of cut, suggesting more balanced surfaces with deeper valleys. Cutting speed had a minor influence, slightly increasing the skewness at low feed rates due to finer peak formation, though this trend was inconsistent at higher feeds. Feed per tooth had the most pronounced effect. At 0.8 mm/rev, the R_{sk} and S_{sk} values were highest, while at 1.6 mm/rev, they decreased, indicating a shift toward more symmetrical distributions. This change was attributed to more aggressive material removal and broader feed marks, which reduce peak sharpness.

Kurtosis parameters (R_{ku} and S_{ku}), which describe the peakedness of the surface, ranged between 2.29 and 2.64. Higher values were associated with low feed and high cutting speed, indicating sharper, isolated peaks. For example, the highest R_{ku} and S_{ku} were recorded at 0.8 mm/rev, 400 m/min, and 0.6 mm depth under dry conditions. As the feed and depth increased, these values declined, confirming that heavier machining produces flatter, more plateau-like surfaces. These trends support the interpretation that cutting conditions directly influence the surface symmetry and peak characteristics, which are critical for tribological performance.

Regarding lubrication, the application of coolant consistently led to decreases in the R_{sk}, S_{sk}, R_{ku}, and S_{ku} values, particularly under low-feed, low-depth setups. At 0.8 mm/rev and 0.3 mm depth, R_{sk} dropped from 0.85 (dry) to 0.60 (wet), while S_{sk} decreased from 0.85 to 0.61, reflecting a shift toward more symmetric surfaces with less peak dominance. Likewise, R_{ku} dropped from 2.35 to 2.04, and S_{ku} from 2.48 to 2.05. The average decrease in kurtosis values with lubrication was 0.15–0.30, while the skewness reduced by 0.2–0.3, indicating that lubrication produces smoother, more balanced textures with less extreme height features. This effect was particularly evident at low feed and low depth combinations, where lubrication mitigated built-up edge formation and thermal distortion, thereby suppressing sharp peaks and producing more uniform surfaces. At higher feed and depth values, the difference between dry and wet conditions was less substantial, with R_{sk}/S_{sk} and R_{ku}/S_{ku} changes typically within $\pm$0.05–0.10, confirming that under aggressive cutting, lubrication has a reduced but still measurable effect on topography symmetry.

In summary, higher feed and depth of cut values generally reduced the skewness and kurtosis, indicating less peaky, more uniform surfaces. Cutting speed played a minor role but slightly increased peakedness at lower feeds. The application of flood lubrication consistently reduced both skewness and kurtosis, especially under milder cutting conditions, highlighting its smoothing and balancing effect on the surface texture. These changes in topography symmetry are crucial for applications requiring enhanced tribological behavior such as improved lubricant film formation or reduced frictional resistance.

While the present study provides a comprehensive analysis of cutting forces and surface topography under varying lubrication and cutting conditions, several limitations must be acknowledged. First, the experimental design focused on a limited set of cutting parameters (specifically two levels each of feed per tooth, cutting speed, and depth of cut) which, while representative of industrial practice, may not capture the full spectrum of process variability. Second, the findings are material-specific, based on C45 medium carbon steel, and may not directly generalize to other alloys or hardened steels without further validation. Third, only flood lubrication and dry machining were considered; alternative strategies such as minimum quantity lubrication, cryogenic cooling, or high-pressure coolant systems were not evaluated. Additionally, the study assumed a consistent tool geometry and insert condition throughout the tests, although insert wear was monitored and we managed to minimize its influence. Future research should explore the effects of advanced lubrication techniques, investigate tool wear progression under high-feed conditions, and extend the analysis to different materials and coated inserts. Integrating

real-time thermal imaging and force monitoring could also enhance the predictive modeling of machining outcomes, contributing to more robust process optimization.

4.3. Statistical Analysis of the Results

To complement the factorial analysis and further clarify the individual influence of each setup parameter on the measured responses, Pearson's correlation coefficients were calculated. These results are shown in Tables 5–7. This statistical approach allows for the strength and direction of linear relationships between the machining parameters to be quantified as well as the resulting cutting forces and surface roughness values. This provides an additional view of the trends observed in the experimental results.

Table 5. Pearson's correlation coefficients between the setup parameters and cutting force components.

Variable	$F_{c,max}$ [N]	$F_{f,max}$ [N]	$F_{f,min}$ [N]	$F_{xy,max}$ [N]	$F_{p,max}$ [N]
f_z	0.639	0.587	−0.669	0.638	0.576
v_c	−0.036	−0.240	0.233	−0.034	0.047
a	0.739	0.746	−0.666	0.741	0.811
Q	−0.003	−0.005	0.025	−0.002	0.001

Table 6. Pearson's correlation coefficients between the setup parameters and 2D surface roughness parameters.

Variable	R_a [µm]	R_q [µm]	R_z [µm]	R_p [µm]	R_v [µm]	R_{sk} [-]	R_{ku} [-]
f_z	0.994	0.995	0.997	0.999	0.988	−0.301	−0.184
v_c	−0.006	−0.005	−0.005	0.006	−0.026	0.285	0.267
a	−0.002	−0.002	0.010	0.008	0.013	0.059	0.110
Q	0.102	0.095	0.071	0.044	0.127	−0.760	−0.842

Table 7. Pearson's correlation coefficients between the setup parameters and 3D areal surface topography parameters.

Variable	S_a [µm]	S_q [µm]	S_z [µm]	S_p [µm]	S_v [µm]	S_{sk} [-]	S_{ku} [-]
f_z	0.993	0.994	0.997	0.998	0.988	−0.192	−0.184
v_c	−0.006	−0.006	−0.022	−0.004	−0.060	0.320	0.203
a	0.000	0.000	0.007	0.005	0.013	0.066	0.086
Q	0.106	0.097	0.066	0.052	0.095	−0.750	−0.849

The results clearly demonstrate that the feed per tooth showed the strongest and most consistent correlations with both the cutting force and surface roughness parameters. For the areal roughness measures, correlation coefficients ranged between 0.988 and 0.998, while for the profile parameters, the values were similarly high (0.988–0.999). This indicates an almost perfectly linear relationship: as the feed per tooth increases, the surface roughness parameters increase proportionally, producing a much rougher surface. Likewise, feed per tooth also correlated positively with all major cutting force components, with coefficients between 0.576 and 0.639, while showing a strong negative correlation with $F_{f,min}$ (−0.669). This behavior aligns with the physical expectations of the process. Higher feed rates result in thicker uncut chips, larger contact areas, and thus higher material resistance and cutting forces as well as more pronounced feed marks on the machined surface. The weak negative correlations between f and the skewness/kurtosis parameters (R_{sk}, S_{sk}, R_{ku}, S_{ku}) suggest that while the overall roughness increases, the surface height distribution becomes slightly more symmetric and less peaked, which is typical for high-feed conditions where deeper valleys and shallower peaks coexist. In contrast, cutting speed demonstrated negligible

correlations with almost all measured quantities, with coefficients typically between −0.02 and +0.32. This indicates that within the tested range (200–400 m/min), the cutting speed exerted only a minimal effect on both the surface topography and cutting forces. This observation is consistent with previous findings in high-feed milling, where chip thickness and feed dominate the mechanical response, while moderate speed variations mainly influence the thermal effects, which are less significant under efficient chip evacuation and short contact times. The slightly positive correlation between v_c and the skewness/kurtosis parameters (R_{sk}, R_{ku}, S_{sk}, S_{ku}) may indicate small changes in the shape of surface asperities at higher cutting speeds, possibly due to minor thermal smoothing effects, but the impact remains limited.

The depth of cut showed a slightly positive correlation with all cutting force components (0.739–0.811), which confirms its role in determining the overall material removal rate and the corresponding mechanical load. However, the correlation between depth of cut and roughness parameters was very weak (close to zero), implying that within the examined range (0.3–0.6 mm), the effect of axial engagement on surface finish was secondary to that of feed per tooth. Depth of cut primarily increased the volume of material removed but did not substantially alter the feed mark geometry or surface asperity distribution.

Finally, the lubrication flow rate exhibited distinct negative correlations with the surface skewness and kurtosis parameters (R_{sk}, S_{sk}: approximately −0.75; R_{ku}, S_{ku}: approximately −0.84), suggesting that lubrication promotes smoother and more plateau-like surface structures by reducing the prominence of sharp peaks. For other roughness and force parameters, the correlations were weak (within ±0.13), indicating that the effect of lubrication on general force magnitudes and average roughness values is relatively minor. Instead, its influence appears more pronounced in modifying the microgeometry of the surface, promoting tribologically favorable textures.

Overall, the correlation analysis confirmed that feed per tooth is the dominant factor governing both mechanical and surface responses in high-feed face milling. Depth of cut significantly affects the force levels but not roughness, while the cutting speed and lubrication mainly fine-tune the process through secondary thermal and surface effects.

Alongside the Pearson's correlation coefficients, ANOVA tests were conducted for selected parameters to complement the statistical evaluation of the results (Tables 8–11). While correlation analysis quantifies linear relationships between individual parameters and measured outcomes, ANOVA identifies the statistical significance of main factors and their interactions, thereby revealing which machining parameters most strongly influence the surface and force characteristics. The ANOVA results showed clear distinctions among the tested variables. For the areal roughness parameter S_q, the feed per tooth and lubrication flow rate showed highly significant effects ($p < 0.001$), confirming their dominant roles in shaping the surface texture. The interaction between feed and lubrication ($f_z \times Q$) was also statistically significant ($p < 0.001$), indicating that the influence of feed on surface roughness is dependent on whether the process is dry or lubricated. In contrast, cutting speed (v_c) and other higher-order interactions had no significant effect, consistent with the correlation findings showing negligible relationships between speed and roughness.

In the case of surface skewness, again, the lubrication flow rate had the strongest effect ($p < 0.001$), followed by significant influences of cutting speed ($p = 0.006$) and its interaction with feed ($p = 0.007$). These results suggest that both the lubrication system and speed jointly affect the height distribution symmetry of the surface, with coolant application leading to more balanced, less peak-dominated textures. Similarly, surface kurtosis was strongly affected by lubrication ($p < 0.001$), while both feed ($p = 0.033$) and cutting speed ($p = 0.022$) also reached statistical significance. The interaction between feed and lubrication ($f_z \times Q$) was again important ($p = 0.001$), reinforcing that coolant modifies the surface height distribution in combination with feed intensity. For the resultant in-plane cutting force,

only the feed per tooth had a statistically significant influence (p = 0.047), while neither cutting speed, lubrication, nor their interactions had any measurable effect. This outcome corroborates the experimental observations that material engagement, affected by feed, dominates force generation during high-feed milling.

Table 8. ANOVA results for the areal root mean square roughness parameter (S_q).

Cases	Sum of Squares	Degrees of Freedom	Mean Square	F Value	p Value
f_z	308.099	1	308.099	74,775.647	<0.001
v_c	0.012	1	0.012	3.004	0.121
Q	2.918	1	2.918	708.227	<0.001
$f_z \times v_c$	0.003	1	0.003	0.754	0.41
$f_z \times Q$	0.493	1	0.493	119.689	<0.001
$v_c \times Q$	0.001	1	0.001	0.268	0.618
$f_z \times v_c \times Q$	0.002	1	0.002	0.465	0.515
Residuals	0.033	8	0.004		

Table 9. ANOVA results for the areal skewness parameter (S_{sk}).

Cases	Sum of Squares	Degrees of Freedom	Mean Square	F Value	p Value
f_z	0.006	1	0.006	4.874	0.058
v_c	0.017	1	0.017	13.512	0.006
Q	0.093	1	0.093	74.076	<0.001
$f_z \times v_c$	0.017	1	0.017	13.221	0.007
$f_z \times Q$	0.018	1	0.018	14.414	0.005
$v_c \times Q$	0.001	1	0.001	1.197	0.306
$f_z \times v_c \times Q$	0.003	1	0.003	2.494	0.153
Residuals	0.01	8	0.001		

Table 10. ANOVA results for the areal kurtosis parameter (S_{ku}).

Cases	Sum of Squares	Degrees of Freedom	Mean Square	F Value	p Value
f_z	0.014	1	0.014	6.622	0.033
v_c	0.017	1	0.017	8.034	0.022
Q	0.306	1	0.306	140.973	<0.001
$f_z \times v_c$	0.019	1	0.019	8.867	0.018
$f_z \times Q$	0.049	1	0.049	22.548	0.001
$v_c \times Q$	0.0005739	1	0.0005739	0.264	0.621
$f_z \times v_c \times Q$	0.0007864	1	0.0007864	0.362	0.564
Residuals	0.017	8	0.002		

Table 11. ANOVA results for the maximum planar cutting force component ($F_{xy,max}$).

Cases	Sum of Squares	Degrees of Freedom	Mean Square	F Value	p Value
f_z	1,178,000	1	1,178,000	5.522	0.047
v_c	3412.07	1	3412.07	0.016	0.902
Q	17.77	1	17.77	0.000083	0.993
$f_z \times v_c$	283.13	1	283.13	0.001	0.972
$f_z \times Q$	870.91	1	870.91	0.004	0.951
$v_c \times Q$	1062.37	1	1062.37	0.005	0.945
$f_z \times v_c \times Q$	50.58	1	50.58	0.00023	0.988
Residuals	1,706,000	8	213,234.65		

Overall, the ANOVA analysis confirms that feed per tooth and lubrication flow rate are the two primary factors influencing both the surface roughness and force behavior, while cutting speed plays a minor or negligible role within the investigated parameter range. The significant interactions between feed and lubrication highlight the coupled tribological and mechanical effects that govern the surface formation mechanisms in high-feed milling.

5. Conclusions

This study investigated the influence of cutting parameters and lubrication on the performance of the high-feed face milling of C45 medium carbon steel. A systematic experimental approach was applied, using a full factorial design encompassing variations in feed per tooth, cutting speed, axial depth of cut, and lubrication condition. Cutting forces were measured using a three-component dynamometer, while the machined surface topography was analyzed using both profile and areal roughness parameters. The combined analysis of cutting forces and surface quality enables a comprehensive understanding of the interplay between process parameters, lubrication, and their effects on machining performance.

The experimental results confirm that feed per tooth is the most influential factor affecting both the cutting forces and surface roughness in the high-feed face milling of C45 steel. Increasing the feed rate led to significant rises in tangential, thrust, and feed-directional forces as well as in the surface texture parameters. These effects were consistent across both the dry and flood-lubricated conditions, highlighting the strong correlation between material engagement and tool load. Axial depth of cut was the second most significant parameter, contributing to increased cutting forces and roughness, though to a lesser extent than feed. Doubling the depth of cut notably amplified the force magnitudes and surface errors, especially in combination with high feed rates. Cutting speed had a comparatively minor effect, slightly reducing the peak forces and roughness due to thermal softening and reduced friction, but did not significantly alter the force fluctuations. Flood lubrication contributed to more consistent cutting conditions. While its quantitative impact on force and roughness was modest (typically within 1–5%), it consistently reduced the force variation and improved surface uniformity. Lubrication also promoted more symmetric surface profiles, as indicated by reductions in the skewness and kurtosis parameters.

Overall, the study demonstrates a clear link between the cutting parameters and surface integrity. Higher feed and depth increase the tool load and roughness, while lubrication supports consistent machining behavior and surface consistency. These insights support the optimization of high-feed milling operations for improved productivity and tribological performance.

Based on these findings, the following novel contributions to the field of machining and tribology can be highlighted:

1. This study demonstrates a clear quantitative relationship between feed per tooth, depth of cut, and both cutting forces and surface roughness, providing a dataset directly linking high-feed milling parameters to tribological outcomes.
2. While lubrication is widely acknowledged to reduce friction, this work provides precise measurements of its effects on the peak cutting forces, force fluctuations, and surface roughness parameters. Flooded coolant reduced the peak forces by 1–5% and decreased the valley depths by up to 17%, highlighting its improving influence in high-feed milling scenarios.
3. The study confirms that feed per tooth is the most influential factor on both forces and surface roughness, followed by depth of cut, while cutting speed has secondary effects. This hierarchy provides guidance for process optimization in terms of productivity, surface quality, and tribological performance.

The results also point to several ways for future research. First, the influence of different lubrication strategies, such as minimum quantity lubrication (MQL), cryogenic cooling, or nanofluid-based lubricants, could be explored to assess their potential for further force reduction and surface improvement. Second, investigations on tool wear progression under high-feed milling with dry and lubricated conditions would provide insights into tool life and maintenance requirements. Third, an extension of this study to different steel grades and coated inserts could help generalize the findings and provide industry-relevant recommendations. Finally, integrating high-resolution thermal imaging and in-process force monitoring could enable the development of predictive models linking machining parameters, lubrication, cutting forces, and surface topography.

In summary, this work provides a detailed experimental evaluation of the high-feed face milling of C45 steel, demonstrating the combined effects of feed, speed, depth, and lubrication on the cutting forces and surface roughness. Feed per tooth emerged as the primary driver of both the cutting load and surface quality, while axial depth of cut contributed moderately, and cutting speed played a minor role. Flood lubrication stabilizes the cutting forces and slightly improves surface uniformity, while dry machining leads to higher forces and more pronounced surface irregularities. These findings provide a quantitative basis for optimizing high-feed face milling operations in terms of productivity, surface quality, and tribological performance.

Author Contributions: Conceptualization, G.V. and I.S.; Methodology, G.V., I.S. and A.N.; Software, G.V.; Validation, G.V. and I.S.; Formal analysis, G.V., I.S. and A.N.; Investigation, G.V., I.S. and A.N.; Resources, G.V. and I.S.; Data curation, I.S. and A.N.; Writing—original draft preparation, G.V., I.S. and A.N.; Writing—review and editing, G.V. and I.S.; Visualization, G.V., I.S. and A.N.; Supervision, G.V. and I.S.; Project administration, G.V.; Funding acquisition, G.V. All authors have read and agreed to the published version of the manuscript.

Funding: This research received no external funding.

Data Availability Statement: The original contributions presented in the study are included in the article; further inquiries can be directed to the corresponding author.

Conflicts of Interest: The authors declare no conflicts of interest.

References

1. Pervaiz, S.; Kannan, S.; Deiab, I.; Kishawy, H. Role of Energy Consumption, Cutting Tool and Workpiece Materials towards Environmentally Conscious Machining: A Comprehensive Review. *Proc. Inst. Mech. Eng. Part B J. Eng. Manuf.* **2019**, *234*, 335–354. [CrossRef]
2. Pawanr, S.; Gupta, K. A Review on Recent Advances in the Energy Efficiency of Machining Processes for Sustainability. *Energies* **2024**, *17*, 3659. [CrossRef]
3. Yusuf, L.A.; Popoola, K.; Musa, H. A Review of Energy Consumption and Minimisation Strategies of Machine Tools in Manufacturing Process. *Int. J. Sustain. Eng.* **2021**, *14*, 1826–1842. [CrossRef]
4. Diaz, N.; Redelsheimer, E.; Dornfeld, D. Energy Consumption Characterization and Reduction Strategies for Milling Machine Tool Use. In *Glocalized Solutions for Sustainability in Manufacturing: Proceedings of the 18th CIRP International Conference on Life Cycle Engineering, Technische Universität Braunschweig, Braunschweig, Germany, 2–4 May 2011*; Springer: Berlin/Heidelberg, Germany, 2011; pp. 263–267.
5. Abdelaoui, F.Z.E.; Jabri, A.; Barkany, A.E. Optimization Techniques for Energy Efficiency in Machining Processes—A Review. *Int. J. Adv. Manuf. Technol.* **2023**, *125*, 2967–3001. [CrossRef]
6. Saı, W.B.; Salah, N.B.; Lebrun, J.L. Influence of Machining by Finishing Milling on Surface Characteristics. *Int. J. Mach. Tools Manuf.* **2001**, *41*, 443–450. [CrossRef]
7. Khorasani, A.M.; Yazdi, M.R.S.; Safizadeh, M.S. Analysis of Machining Parameters Effects on Surface Roughness: A Review. *Int. J. Comput. Mater. Sci. Surf. Eng.* **2012**, *5*, 68. [CrossRef]
8. Baradie, M.A.E. Cutting Fluids: Part I. Characterisation. *J. Mater. Process. Technol.* **1996**, *56*, 786–797. [CrossRef]

9. Wu, C.-H.; Chien, C.-H. Influence of Lubrication Type and Process Conditions on Milling Performance. *Proc. Inst. Mech. Eng. Part B J. Eng. Manuf.* **2007**, *221*, 835–843. [CrossRef]
10. Williams, J.A.; Tabor, D. The Role of Lubricants in Machining. *Wear* **1977**, *43*, 275–292. [CrossRef]
11. Abdelrazek, A.H.; Choudhury, I.A.; Nukman, Y.; Kazi, S.N. Metal Cutting Lubricants and Cutting Tools: A Review on the Performance Improvement and Sustainability Assessment. *Int. J. Adv. Manuf. Technol.* **2020**, *106*, 4221–4245. [CrossRef]
12. Iqbal, A.; Zhao, G.; Cheok, Q.; He, N.; Nauman, M.M. Sustainable Machining: Tool Life Criterion Based on Work Surface Quality. *Processes* **2022**, *10*, 1087. [CrossRef]
13. Sreejith, P.S.; Ngoi, B.K.A. Dry Machining: Machining of the Future. *J. Mater. Process. Technol.* **2000**, *101*, 287–291. [CrossRef]
14. Goindi, G.S.; Sarkar, P. Dry Machining: A Step towards Sustainable Machining—Challenges and Future Directions. *J. Clean. Prod.* **2017**, *165*, 1557–1571. [CrossRef]
15. Dudás, I.; Lierath, F.; Varga, G.Y. *Környezetbarát Technológiák a Gépgyártásban [Environmentally Friendly Technologies in Mechanical Engineering]*; Műszaki Könyvkiadó: Budapest, Hungary, 2010; 308p, ISBN 978-963-166-500-0. (In Hungarian)
16. Debnath, S.; Reddy, M.M.; Yi, Q.S. Environmental Friendly Cutting Fluids and Cooling Techniques in Machining: A Review. *J. Clean. Prod.* **2014**, *83*, 33–47. [CrossRef]
17. Maruda, R.W.; Krolczyk, G.M.; Nieslony, P.; Wojciechowski, S.; Michalski, M.; Legutko, S. The Influence of the Cooling Conditions on the Cutting Tool Wear and the Chip Formation Mechanism. *J. Manuf. Process.* **2016**, *24*, 107–115. [CrossRef]
18. Schoop, J. In-Situ Calibrated Modeling of Residual Stresses Induced in Machining under Various Cooling and Lubricating Environments. *Lubricants* **2021**, *9*, 28. [CrossRef]
19. Biermann, D.; Saelzer, J.; Bergmann, B.; Schenzel, J.; Menze, C.J.; Gerken, J.F.; Wolf, T.; Denkena, B.; Möhring, H.-C.; Zabel, A. Fundamental Characterization of Lubrication Effects through Various Cooling Lubricants in the Chip Formation Zone. *Prod. Eng.* **2024**, *19*, 173–185. [CrossRef]
20. Varghese, V.; Ramesh; Chakradhar, D. Experimental Investigation and Optimization of Machining Parameters for Sustainable Machining. *Mater. Manuf. Process.* **2018**, *33*, 1782–1792. [CrossRef]
21. Paturi, U.M.R.; Yash, A.; Palakurthy, S.T.; Reddy, N.S. Modeling and Optimization of Machining Parameters for Minimizing Surface Roughness and Tool Wear during AISI 52100 Steel Dry Turning. *Mater. Today Proc.* **2021**, *50*, 1164–1172. [CrossRef]
22. Davoodi, B.; Tazehkandi, A.H. Experimental Investigation and Optimization of Cutting Parameters in Dry and Wet Machining of Aluminum Alloy 5083 in Order to Remove Cutting Fluid. *J. Clean. Prod.* **2014**, *68*, 234–242. [CrossRef]
23. Li, S.; Wang, X.; Xie, L.; Pang, S.; Peng, S.; Liang, Z.; Jiao, L. The Milling–Milling Machining Method and Its Realization. *Int. J. Adv. Manuf. Technol.* **2014**, *76*, 1151–1161. [CrossRef]
24. Karpuschewski, B.; Byrne, G.; Denkena, B.; Oliveira, J.; Vereschaka, A. Machining Processes. In *Springer Handbook of Mechanical Engineering*; Springer: Cham, Switzerland, 2021; pp. 409–460.
25. Jiang, Y.; Yang, X.; Tian, H.; Ma, L.; Li, L.; Yang, Y. Investigation on the High-Feed Milling of M28. *Int. J. Adv. Manuf. Technol.* **2023**, *129*, 127–141. [CrossRef]
26. Kuruc, M.; Vozar, M.; Simna, V.; Vopat, T.; Hrusecky, R.; Milde, J. Comparison of High Feed Machining with Conventional Milling in Terms of Dimension Accuracy and Productivity. In Proceedings of the 29th DAAAM International Symposium on Intelligent Manufacturing and Automati, Zadar, Croatia, 24–27 October 2018; pp. 426–434.
27. Borysenko, D.; Kundrák, J.; Karpuschewski, B.; Welzel, F.; Maros, Z.; Felhő, C. Surface Residual Stresses in High-Feed Face Milling of Carbon Steel. In *Lecture Notes in Mechanical Engineering*; Springer: Cham, Switzerland, 2022; pp. 648–653.
28. Płodzień, M.; Żyłka, Ł.; Sułkowicz, P.; Żak, K.; Wojciechowski, S. High-Performance Face Milling of 42CRMO4 Steel: Influence of Entering Angle on the Measured Surface Roughness, Cutting Force and Vibration Amplitude. *Materials* **2021**, *14*, 2196. [CrossRef]
29. Zhao, P.; Cheng, K.; Jiang, B.; Zuo, L. Development of the Innovative Differential Tool Wear Modeling for High-Feed Milling and Its Experimental Verification. *Proc. Inst. Mech. Eng. Part B J. Eng. Manuf.* **2020**, *235*, 85–97. [CrossRef]
30. Russo, D.; Urbicain, G.; Egea, A.J.S.; Simoncelli, A.; Krahmer, D.M. Milling Force Model for Asymmetric End-Mills during High-Feed Milling on AISI-P20. *Mater. Manuf. Process.* **2021**, *36*, 1761–1768. [CrossRef]
31. Karpuschewski, B.; Kundrák, J.; Varga, G.; Deszpoth, I.; Borysenko, D. Determination of Specific Cutting Force Components and Exponents When Applying High Feed Rates. *Procedia CIRP* **2018**, *77*, 30–33. [CrossRef]
32. Pálmai, Z.; Kundrák, J.; Felhő, C.; Makkai, T. Investigation of the Transient Change of the Cutting Force during the Milling of C45 and X5CrNi18-10 Steel Taking into Account the Dynamics of the Electro-Mechanical Measuring System. *Int. J. Adv. Manuf. Technol.* **2024**, *133*, 163–182. [CrossRef]
33. Jacquet, T.; Fromentin, G.; Prat, D.; Viprey, F. Modeling of High-Feed Milling and Surface Quality Applied to Inconel 718. *Procedia CIRP* **2024**, *123*, 113–118. [CrossRef]
34. Kundrak, J.; Felho, C. Topography of the Machined Surface in High Performance Face Milling. *Procedia CIRP* **2018**, *77*, 340–343. [CrossRef]
35. Nagy, A.; Kundrák, J. Roughness of Face-Milled Surface Topography in Directions Relative to the Feed Movement. *Manuf. Technol.* **2024**, *24*, 241–254. [CrossRef]

36. Taguchi, G. *System of Experimental Design: Engineering Methods to Optimize Quality and Minimize Costs*; Unipub/Kraus International Publications: White Plains, NY, USA, 1987; 1189p, ISBN 978-052-791-621-3.
37. Fridrik, L. *Válogatott Fejezetek a Gépgyártástechnológiai Kísérletek Tervezése Témaköréből [Selected Chapters on the Topic of Designing Engineering Technology Experiments]*; Tankönyvkiadó: Budapest, Hungary, 1993. (In Hungarian)
38. Ishfaq, K.; Anjum, I.; Pruncu, C.I.; Amjad, M.; Kumar, M.S.; Maqsood, M.A. Progressing towards Sustainable Machining of Steels: A Detailed Review. *Materials* **2021**, *14*, 5162. [CrossRef] [PubMed]
39. Nair, A.; Kumanan, S.; Prakash, C.; Mohan, D.G.; Saxena, K.K.; Kumar, S.; Kumar, G. Research Developments and Technological Advancements in Conventional and Non-Conventional Machining of Superalloys—A Review. *J. Adhes. Sci. Technol.* **2023**, *37*, 3053–3124. [CrossRef]
40. Yin, Q.; Li, C.; Dong, L.; Bai, X.; Zhang, Y.; Yang, M.; Jia, D.; Li, R.; Liu, Z. Effects of Physicochemical Properties of Different Base Oils on Friction Coefficient and Surface Roughness in MQL Milling AISI 1045. *Int. J. Precis. Eng. Manuf.-Green Technol.* **2021**, *8*, 1629–1647. [CrossRef]
41. Pimenov, D.Y.; Abbas, A.T.; Gupta, M.K.; Erdakov, I.N.; Soliman, M.S.; Rayes, M.M.E. Investigations of Surface Quality and Energy Consumption Associated with Costs and Material Removal Rate during Face Milling of AISI 1045 Steel. *Int. J. Adv. Manuf. Technol.* **2020**, *107*, 3511–3525. [CrossRef]
42. Upadhyay, C.; Rajput, S.S.; Bera, S.; Ju, H.; Bhide, R.; Gangopadhyay, S. Influence of TiAlN Coating Thickness in Dry Machining of AISI 1045 Steel Using Finite Element Simulation and Experiments. *Surf. Coat. Technol.* **2024**, *495*, 131496. [CrossRef]
43. Baldin, V.; Da Silva, L.R.R.; Davis, R.; Jackson, M.J.; Amorim, F.L.; Houck, C.F.; Machado, Á.R. Dry and MQL Milling of AISI 1045 Steel with Vegetable and Mineral-Based Fluids. *Lubricants* **2023**, *11*, 175. [CrossRef]
44. Saleem, M.Q.; Mumtaz, S. Face Milling of Inconel 625 via Wiper Inserts: Evaluation of Tool Life and Workpiece Surface Integrity. *J. Manuf. Process.* **2020**, *56*, 322–336. [CrossRef]
45. Muthuswamy, P.; Nagarajan, S.K. Experimental Investigation on the Effect of Different Micro-Geometries on Cutting Edge and Wiper Edge on Surface Roughness and Forces in Face Milling. *Lubricants* **2021**, *9*, 102. [CrossRef]
46. Borysenko, D.; Karpuschewski, B.; Welzel, F.; Kundrák, J.; Felhő, C. Influence of Cutting Ratio and Tool Macro Geometry on Process Characteristics and Workpiece Conditions in Face Milling. *CIRP J. Manuf. Sci. Technol.* **2019**, *24*, 1–5. [CrossRef]
47. Zhang, P.R.; Liu, Z.Q.; Guo, Y.B. Machinability for Dry Turning of Laser Cladded Parts with Conventional vs. Wiper Insert. *J. Manuf. Process.* **2017**, *28*, 494–499. [CrossRef]
48. Kurniawan, D.; Yusof, N.M.; Sharif, S. Hard Machining of Stainless Steel Using Wiper Coated Carbide: Tool Life and Surface Integrity. *Mater. Manuf. Process.* **2010**, *25*, 370–377. [CrossRef]
49. Muthuswamy, P. A Novel Wiper Insert Design and an Experimental Investigation to Compare Its Performance in Face Milling. *Adv. Mater. Process. Technol.* **2022**, *8*, 2070–2085. [CrossRef]
50. *ISO 25178:2012*; Geometrical Product Specifications (GPS)—Surface Texture: Areal. International Organization for Standardization: Geneva, Switzerland, 2012.
51. Gadelmawla, E.S.; Koura, M.M.; Maksoud, T.M.A.; Elewa, I.M.; Soliman, H.H. Roughness Parameters. *J. Mater. Process. Technol.* **2002**, *123*, 133–145. [CrossRef]

Disclaimer/Publisher's Note: The statements, opinions and data contained in all publications are solely those of the individual author(s) and contributor(s) and not of MDPI and/or the editor(s). MDPI and/or the editor(s) disclaim responsibility for any injury to people or property resulting from any ideas, methods, instructions or products referred to in the content.